Integrative multi-omic and phenotypic analysis of open raceway pond production of *Monoraphidium minutum* 26B-AM reveals distinct stress signatures for scale-up and infection.

Georgios Kepesidis [a], Jenna Schambach [b], Daniel Yang [a], Elise Wilbourn [c], Thomas Sheffield [a], Tyler Eckles [c], Olivia Watt [c], Matthew P. Hirakawa [a], Todd W. Lane [c], Raga Krishnakumar [a+]

a Biosecurity and Bioassurance, Sandia National Laboratories, Livermore, 94550, U.S.A.

b Environmental Systems Biology, Sandia National Laboratories, Albuquerque, 87123, U.S.A.

c Bioresource & Environmental Security, Sandia National Laboratories, Livermore, 94550, U.S.A.

+ Corresponding author

Abstract

Background: Green microalgae, such as *Monoraphidium minutum* 26B-AM, have garnered significant commercial interest due to their high biomass production and lipid yield, providing promising candidates for various bioprocessing applications. However, the economic viability of large-scale algal cultivation in open raceway ponds is limited by biocontamination and environmental stressors, necessitating deeper understanding of the molecular mechanisms that underpin resilience and productivity in these systems. We hypothesized that the molecular signature associated with the cellular responses of *M. minutum* to environmental stressors will reveal critical information for the timely prediction of resilience and productivity in algal cultures within open pond systems.

Results: To test this hypothesis, we conducted a longitudinal multi-omic study, integrating transcriptomics, proteomics, metabolomics, and phenomics, to monitor the acclimation, growth dynamics, and pathogen responses of algal cultures in two 1000 L raceway ponds, before and after the introduction of a pathogen as a stressor. We identified a number of molecular patterns that correlate with changes in the algal environment, and we can track these changes within the ponds per time. Furthermore, we identify scale-up and infection-specific molecular pathways through integrated multi-omics, showing that most patterns are unique to each studied stressor/transition.

Conclusions: Ultimately, this study demonstrates the utility of multi-omics observations at scale, revealing unique signatures and laying the groundwork for developing molecular detection techniques and predictive models that can improve the sustainability and efficiency of large-scale algae biomass production.

Keywords

Multi-omics, algae, *Monoraphidium minutum*, ponds, transcriptomics, metabolomics, proteomics, biomarkers

1. Background

Microalgae are a polyphyletic group of unicellular photosynthetic aquatic organisms that have attracted commercial interest since the middle of the past century because of their potential to advance biotechnology and biomanufacturing processes. Compared to land plants, their biomass yield is greater [1], and their high content of useful metabolites, such as lipids, has increased their presence in multiple industrial bioprocesses, including the production of food, pharmaceuticals, cosmetics, bioplastics, and biofuels. The high production costs, however, curtail most of these applications, especially for low-cost and high-volume products such as biofuels, making the use of algae currently unfeasible and unsustainable and restricting their potential [2] [3] [4].

A low-energy and low-cost method for large-scale production of algal biomass, given the financial restrictions for algal cultivation mentioned earlier, is the paddlewheel-based open raceway pond cultivation system [5] [6]. These widely used systems allow the cultures to grow in direct relation to the

surrounding environment and the local weather conditions. Additionally, these ponds can be established on land that is not suitable for terrestrial agriculture, thereby utilizing a resource that would otherwise remain unused.

Despite their advantages, a number of barriers preclude the overall economic viability of bioprocesses within these systems. One crucial barrier is the susceptibility of the cultures to environmental "intruders", which threaten both the quality of the final product and the overall survival of the pond cultures [7]. These events lead to pond crashes and a significant increase in operational costs, strongly establishing the need for their timely prediction.

In combination with the growth of undesired microbial organisms, open pond systems are susceptible to unpredictable changes in the weather [8], as are other site-specific environmental factors, such as sand particles or dust, which change the composition of the culture media [9]. All these factors, which are directly related to the immediate exposure of the cultures to their biotic and abiotic surroundings, can lead to unpredictable outcomes in terms of biomass productivity [10]. In addition, the growth and productivity are not always aligned with the observations made at smaller scales [11]. Understanding the effects that all these variables have on culture outcomes is critical to optimally predict growth in industrial settings. Consequently, optimal prediction can guide the design of resilient culture systems, ultimately reducing the cost of each operation. Identification of exposure- and threat-agnostic biomarkers of stress as expressed by the microalgae themselves would allow for detailed monitoring and remediation of open cultures in real-time and understanding what molecular pathways might be involved in resilience.

In the current industrial landscape, enhancing the resilience of expansive open pond systems and optimizing our predictive tools are essential for maintaining the stability of algal production. Here, we utilized cells as sensors of their environment by performing an in-depth multi-omics analysis (transcriptomics, proteomics, metabolomics and phenomics) in order to further understand the molecular dynamics behind the acclimation, growth, and response to infection by a parasitoid amoeboaphelid species (PL3) that are known to cause pond crashes, in two 1000 L open raceway ponds under environmentally-simulated conditions. For this study, we used the freshwater green microalga *Monoraphidium minutum* 26B-AM, a species currently studied as a promising winter species for biofuel feedstock because of its elevated lipid yield [12] [13] [14] [15] [16]. The genome of *M. minutum* has also been recently annotated [17]. [18, 19] Our work reveals a number of molecular signatures and regulatory elements of interest, and lays the groundwork for proactive interventions that can sustain algal health and performance in the face of environmental challenges. In this study, in addition to phenotypical observations, molecular markers evaluated via multi-omics are indicative of distinct stages of open pond culture. We verified this method by demonstrating a known link between light and redox signaling and photosynthesis and translation-related genes in *M. minutum*, in accordance with similar observations in closely related green algal species, confirming the applicability of the markers identified here across algal culture systems. Finally, we focused on the molecular pathways associated with the scale-up acclimation and the introduction of the pathogen into the system through integrated multi-omic analysis. While specific molecular networks of genes, proteins and metabolites were identified for each transition, we discovered unique signatures in response to the two stressors, revealing distinct signaling outcomes across stressors.

2. Methods

114

115 *2.1 Strain and conditions*

116

117 The *M. minutum* 26B-AM strain was initially collected and isolated as described previously [20], and it has
118 been utilized in our laboratory as part of the DISCOVR strain library. Seed cultures of *M. minutum* (100
119 mL) were maintained in sterile 250 mL Erlenmeyer flasks, containing DISCOVR medium [20] under a 16:8
120 h light/dark cycle with continuous shaking at 110 rpm in a closed incubator with LED lighting. The light
121 intensity during the light cycle was 100 µmol photons m^{-2} s^{-1} and the temperature was set between a
122 maximum of 30 °C during the light period and a minimum of 23 °C during the dark period. The seed
123 cultures were diluted regularly to maintain exponential phase growth.

124

125 *2.2 Scale-up*

126

127 The culture scale-up is graphically summarized in Fig.1. The seed cultures of *M. minutum* described above
128 were used as inocula for 500 mL cultures grown in 1 L Erlenmeyer flasks. Progressively, the cultures were
129 transitioned to 2 L bottles, 8 L carboys with stirring and air bubbling and 20 L carboys with bubbling. Each
130 step lasted 10–15 days, until the inoculum was dense enough (approximately 2 million cells/mL) to be
131 diluted to the next scale. Up to the 2 L scale, the cultures were grown under the same conditions as the
132 initial seed cultures detailed in the previous section. For the 20 L carboys, the cultures were acclimated to
133 relatively high light intensities (1500 µmol photons m^{-2} s^{-1}). The 20 L carboys were thermally acclimated
134 between 22-28 °C under a 12/12 h dark/light cycle in a water bath, to match the conditions of the next
135 scale.

Fig. 1: M.minutum scale-up. *A) Graphic representation of the scale-up. B) Picture of the 1000L open raceway pond on Day 0 of the culture run, after the inoculation of the media with the precultures.*

2.3 Cultivation and sample collection at the 1000 L opened raceway ponds

The cultures from the 20 L carboys (3 from each pond- total 60 L) were used as inocula for the 1000 L open raceway ponds. The ponds were filled with tap water and the nutrients and salts were added via the modified 10% BG-11 recipe, as described previously [20]. The ponds were operated under a 12 h/12 h dark/light cycle, implemented with LED light panels, placed over the ponds, reaching 1500 µmol photons m^{-2} s^{-1} during the light period, under a sinusoidal light intensity program (measured in closest proximity to the source). The temperature was maintained within a temperature range of 22-28 °C, with the highest temperature being reached in the middle of the light period and the lowest in the middle of the dark period. Temperature control was achieved through a heat-exchanger lining on the walls of the ponds. The cultures were constantly mixed with a mechanical paddlewheel at 20 rpm. The pH was held constant at 7.2 via CO_2 sparging. The cells were grown under these conditions for 5 days and samples for the different omic analyses were collected on a daily basis one hour after the lights were turned on. For the phenotypic analysis, samples were collected across pond depths and locations to ensure that there were no extreme

154 biases that were unaccounted for (more details below in 2.4). For the 'omics datasets, samples were
155 collected from the middle of the raceway ponds, at equal distance from the surface and the bottom of
156 the pond and from the left and the right walls of the pond, under the assumption that this was the most
157 successfully homogenous spot of the culture. The phenotypic and conditional measurements were taken
158 directly after that.

159 On the 5th day of the cultivation, 2/3 of each pond was drained and fresh water with new nutrients was
160 added. In parallel, an inoculum of the parasitoid amoeboaphelid species FDO1 [19] [18] was added at a
161 0.05% volume concentration, in order to study the dynamics of *M.minutum* pond crashes caused by this
162 strain. This specific strain has been isolated by the Arizona Center for Algae Technology and Innovation as
163 the cause of *Monoraphdium minutum* pond crashes, and it has not yet been fully characterized. Under
164 laboratory conditions, it caused *M. minutum* cultures to crash in 4-5 days. The determination of culture
165 crashes was visual, when the ponds had completely transitioned from green to brown.

166

167 *2.4 Phenotypic and conditional measurements*

168

169 All phenotypic and conditional measurements were taken on a daily basis in technical triplicates unless
170 otherwise stated. The cell count and cell size were determined with the Countess™ 3 FL Automated Cell
171 Counter (Thermo Fisher Scientific, Waltham, MA, USA), from a sample collected from the ponds one hour
172 after the lights were turned on (the maximal temperature and light intensity had been reached).

173 To measure chlorophyll fluorescence, 200 µL pond samples in 96-well transparent plates were measured
174 at an excitation wavelength of 450 nm and an emission wavelength of 685 nm with a Spark® Multimode
175 Microplate Reader (TECAN, Männedorf, Switzerland). The chlorophyll content of the ponds is presented
176 in relative units.

177 For the ash-free dry weight (AFDW) measurements, the steps described in [21] were followed.

178 The total carbohydrate concentration was determined via the Total Carbohydrate Quantification Assay
179 (Abcam, Cambridge, UK), following the manufacturer's instructions. Samples were collected from each
180 pond, alongside the samples for the omic analyses.

181 Samples were collected from each pond for the quantification of total H3 histones. This measurement
182 was performed with the Histone H3 Total Quantification Kit (Abcam, Cambridge, UK), following the
183 manufacturer's protocol, and the colorimetric measurements were conducted using the Spark®
184 Multimode Microplate Reader (TECAN, Männedorf, Switzerland).

185 Samples for the determination of caspase activity were also collected. For the estimation of cell lysis and
186 caspase activity, the EnzChek Caspase-3 Assay Kit #1 (Thermo Fisher Scientific, Waltham, MA, USA) was
187 used, with Z-DEVD-AMC as the substrate, according to the manufacturer's protocol. Dissolved oxygen
188 (%DO), pH, conductivity, temperature and light intensity were measured in each pond, immediately after
189 sample collection. For each variable, we took the average of 9 collected data points, three from the
190 surface, three from the middle and three from the bottom of the pond, in order to take into account the
191 depth-based attenuation that is expected in some of those conditions. The %DO and temperature were
192 measured with the Waterproof Dissolved Oxygen Meter Pen (Sper Scientific Direct, Scottsdale, AZ, USA),

193 the pH and conductivity were measured with an Ohaus Starter AB33M1-F pH & Conductivity Bench Meter
194 (Parsippany, NJ, USA), and the light intensity was measured with an LI-1500 Light Sensor Logger (Lincoln,
195 NE, USA).

196

197 *2.5 Community composition analysis*

198

199 Samples were collected in sterile 15 mL Falcon tubes and stored at -20 °C before analysis. Prior to DNA
200 extraction samples were thawed and media was removed by filtering through a filter plate (Cytiva
201 AcroPrep, 3.0/0.2 µm pore size). Cells were resuspended with Zymo Bashing Bead Buffer and DNA was
202 extracted following manufacturer instructions using a Zymo Quick-DNA Fungal/Bacterial 96 kit. Samples
203 were amplified with the following primers: 357F and 783R [22] [23] for the 16S V3-V4 regions and
204 TAReuk454 and TAReukREV3 TAReukREV3 [24] to amplify the 18S V4 region. Samples were indexed using
205 Nextera XT indexes (Illumina, sets A and D) and 192 samples were multiplexed into a 4 nM final library.
206 This library was sequenced using an Illumina MiSeq. Read classification and relative abundance
207 calculations were performed in Python 3.13.5 using Kraken 2 and Bracken [25] [26] [27]. Community
208 members were assigned using the Silva database (version 138.2) [28].

209

210 *2.6 Transcriptomics/ RNA extraction and cDNA library preparation*

211

212 The samples collected for the transcriptomic analyses (5 mL each) were centrifuged after collection at
213 5000 rpm for 2 minutes at 4 °C, and the resulting cell pellets were stored at -20 °C until RNA extraction
214 was performed.

215 To initiate cell lysis, the frozen pellets were thawed on ice and resuspended in 750 µL of Qiagen RLT Buffer
216 supplemented with 1% β-mercaptoethanol from the RNeasy Plant Mini Kit (Qiagen, Hilden, Germany).
217 The resuspended cells were then transferred to 2 mL tubes containing Lysing Matrix Y zirconium oxide
218 beads (MP Biomedicals, Santa Ana, CA, USA). Following a 10-second vortex, the samples were flash-frozen
219 in liquid nitrogen. After thawing on ice, the cells were lysed via a FastPrep-24 bead beater (MP
220 Biomedicals, Santa Ana, CA, USA) for 25 seconds at 40 Hz. The samples were subsequently centrifuged at
221 9000 rpm for 10 minutes at 4 °C, after which the clear supernatant was collected for RNA extraction. RNA
222 was extracted via the RNeasy Plant Mini Kit (Qiagen, Hilden, Germany) according to the manufacturer's
223 protocol. The quantity of RNA was assessed via a NanoDrop™ One (Thermo Scientific, Waltham, MA, USA),
224 whereas its integrity was evaluated via the 4200 TapeStation System (Agilent Technologies, Santa Clara,
225 CA, USA). RNA samples with a RIN value of 6.5 or higher were deemed to have acceptable integrity and
226 were subsequently processed for the cDNA library construction.

227 For the library preparation for RNA sequencing, the KAPA RNA HyperPrep Kit (Roche, Basel, Switzerland)
228 was utilized, following the manufacturer's instructions. cDNAs were ligated with Unique Dual-Indexed
229 Adapters from the KAPA Kit (Roche, Basel, Switzerland). The concentration of each library was determined
230 via a Qubit fluorometer (Thermo Fisher Scientific, Waltham, MA, USA), and quality was assessed via the
231 4200 TapeStation System (Agilent Technologies, Santa Clara, CA, USA). The libraries were pooled in equal

quantities, and the pooled samples were sent for sequencing at Azenta Genewiz, South Plainfield, NJ, USA. The sequencing was performed on an Illumina NextSeq 500/550 (Illumina, Inc., San Diego, USA) using a 75-cycle run for paired-end reads.

Genes were filtered for at least 75% of the values to be above zero, run through principal component analysis (PCA, with 10 components), and a standard scalar was applied to the PCs.

2.7 Proteomics

For the proteomic analysis (protein extraction, sample preparation, mass spectrometry and early data processing), the pond-collected samples were sent to MS Bioworks, Ann Arbor, MI, USA.

For the sample preparation, the cells were washed twice with 1X PBS and lysed in a modified RIPA buffer containing 50 mM Tris HCl (pH 8.0), 150 mM NaCl, 2.0% SDS, 0.1% TX100, and 1X Roche Complete Protease Inhibitor (Roche, Basel, Switzerland). Lysis was performed using 1.4 mm stainless steel beads in a Next Advance Bullet Blender (Next Advance, Troy, NY, USA) for two cycles of 3 minutes each. The samples were then heated to 60 °C for 30 minutes and clarified by centrifugation at 13,200 rpm. Protein was precipitated via trichloroacetic acid (TCA) overnight at -20 °C, after which the pellet was washed and resuspended in a solution of 8 M urea, 50 mM Tris HCl (pH 8.0), and 1X Roche Complete Protease Inhibitor (Roche, Basel, Switzerland). Protein quantification was performed via a Qubit fluorometer (Thermo Fisher Scientific, Waltham, MA, USA), and a pooled sample was created from all the individual samples. For digestion, 2.5 µg of protein was treated overnight with trypsin. The samples were first reduced at room temperature for 1 hour in 12 mM DTT, followed by alkylation for 1 hour at room temperature in 15 mM iodoacetamide. Trypsin was added at an enzyme-to-substrate ratio of 1:20. Each sample was then acidified to 0.3% TFA and subjected to solid-phase extraction (SPE) using a Waters µHLB (Waters, Pleasenton, CA, USA). The SPE process involved activating the matrix with four additions of 500 µL of 70% acetonitrile, equilibrating with four additions of 500 µL of 0.3% TFA, adding the sample, washing the wells with three additions of 500 µL of 0.3% TFA, and eluting in 200 µL followed by an additional 400 µL of 60% acetonitrile in 0.3% TFA. The samples were then frozen at -80 °C and lyophilized overnight.

For the mass spectrometry analysis, 500 ng of each sample was analyzed in triplicate via an LC-MS/MS setup consisting of a Thermo Fisher Vanquish Neo UPLC system (Thermo Fisher Scientific, Waltham, MA, USA) interfaced with a Thermo Fisher Orbitrap Astral (Thermo Fisher Scientific, Waltham, MA, USA). Peptides were loaded onto a trapping column and eluted through a 75 µm analytical column at a flow rate of 350 nL/min, with the column temperature maintained at 55 °C. A 30-minute gradient was used for elution. The mass spectrometer was operated in data-independent acquisition (DIA) mode, capturing full scan MS data at a resolution of 240,000 FWHM over the m/z range of 380-980, followed by 300 sequential 2 m/z precursor isolation windows, with product ions acquired at a resolution of 40,000 FWHM. The maximum ion injection time (IIT) was set to 3.5 ms for DIA, and the normalized collision energy (NCE) was set to 25. An injection of the pooled sample was included at both the beginning and end of the analysis batch.

The initial data processing for the DIA results was performed via DIA-NN (v1.9.1) [29] , which facilitated several key functions: conversion of RAW files to the QUANT format, alignment on the basis of retention

272 times, searching data via an in-silico spectral library generated from the FASTA file and iteratively from
273 the spectral library derived from RAW data, filtering of database search results at a 1% false discovery rate
274 (FDR) for both peptides and proteins, calculation of peak areas for detected peptides, and normalization
275 of the data. The data were subjected to percentile normalization for the PCA plots.

276

277 *2.8 Metabolomics*

278

279 For the metabolomics analysis of the ponds, 1 mL from the samples taken (containing both the media and
280 cells) was sent to Creative Proteomics, Shirley, NY, USA, for untargeted metabolomics analysis. For the
281 blank, samples with only media were taken from the ponds before the algal inoculation. For the sample
282 preparation, the samples were transferred into a tube for lyophilization. Following transfer, 500 µL of 80%
283 methanol was added, and the mixture was vortexed for 30 seconds and then subjected to sonication in
284 an ice-water bath for 30 minutes. The samples were subsequently stored at -20 °C for 1 hour, after which
285 they were vortexed for an additional 30 seconds and centrifuged at 12,000 rpm for 10 minutes at 4 °C, to
286 lyse and remove the cells. From the resulting supernatant, 200 µL was transferred into a vial, and 5 µL of
287 a 0.14 mg/mL solution of DL-o-chlorophenylalanine was added. The final solution was filtered through a
288 0.22 µm filter in preparation for LC-MS analysis. The separation of the compounds was achieved via the
289 Vanquish Flex UPLC system in conjunction with a Q Exactive Plus mass spectrometer (Thermo Scientific,
290 Waltham, MA, USA), which featured a heated electrospray ionization (ESI) source. The LC separation
291 utilized a Hypersil Gold C18 column (100 × 2.0 mm, 1.9 µm), with the mobile phase consisting of solvent
292 A (0.05% formic acid in water) and solvent B (acetonitrile) under a gradient elution profile: from 0 to 1
293 minute at 5% B, from 1 to 12.5 minutes increasing from 5% to 95% B, holding at 95% B from 12.5 to 13.5
294 minutes, returning to 95% B from 13.5 to 13.6 minutes, and finally returning to 5% B from 13.6 to 16
295 minutes. The flow rate was maintained at 0.3 mL/min, with the column temperature set at 40 °C and the
296 sample manager temperature at 4 °C. The mass spectrometry parameters for both ESI positive (ESI+) and
297 negative (ESI-) modes were configured as follows: for ESI+, the heater temperature was set to 300 °C, the
298 sheath gas flow rate was 45 arb, the auxiliary gas flow rate was 15 arb, the sweep gas flow rate was 1 arb,
299 the spray voltage was 3.0 kV, the capillary temperature was 350 °C, and the S-Lens RF level was 30%. For
300 ESI-, the heater temperature remained at 300 °C, with the same sheath and auxiliary gas flow rates as
301 those used for ESI+, but the spray voltage was adjusted to 3.2 kV, and the S-Lens RF level was increased
302 to 60%. For the bioinformatic analysis (see section 2.9), we considered the metabolites whose abundance
303 was more than 10x greater than the abundance of the metabolites in the blank to be significant.

304 For the small-scale metabolomics, 100 mL cultures of *M.minutum* were grown in 250 mL Erlenmeyer flasks
305 (in triplicate) under the same conditions and media described in 2.1. On day 5 the cultures have been 2/3
306 diluted and FDO1 [19] [18] was added at a 0.05% volume concentration. Samples of 5ml from each flask
307 were collected on days 0, 3, 4, 5, 7, 10, 11, 12, 17 and 18. The LC-MS and bioinformatic analysis were
308 conducted as described for the pond samples.

309

310 *2.9 Bioinformatics*

311

Principal component analysis (PCA) was performed in R with the factoextra package [30]. For 3D PCA analysis, the first 3 components were plotted for each replicate per day, and the centroid point was also plotted on the same axes. Day-specific standard deviation from the centroid (based on replicates) is shown by a shaded sphere.

For RNA sequencing analysis, the following sequence processing steps and associated packages were used: the fastq file was quality-checked with FastQC, and adapter trimming was performed with Trimmomatic [31], t

The pseudoalignment of the transcripts to the transcriptome of *M. minutum* (as it was published and publicly available by [17]) and the quantification of their abundance were performed with the Kallisto package [32]. The integration of the Kallisto data and the differential gene expression analysis, including the time course analysis, was performed with Sleuth [33]. The GEMMA package [34] was used for the correlation of the gene expression with specified quantitative phenotypes.

Additional tools for the multi-omic analyses include ggplot2 [35] for graphic representation and pheatmap [36] for the heatmap.

De novo motif enrichment analysis of the promoter regions (200 bps upstream of ATG) was performed with the Homer Motif Discovery and Analysis software [37].

We used the Data Integration Analysis for Biomarker Discovery using Latent variable approaches for Omics studies (DIABLO) framework from the R software package mixOmics (version 6.28.0) to combine the transcriptomics, proteomics, and metabolomics datasets [38]. Specifically, we compared these data across Day 0 and Day 1 and subsequently Day 4 and Day 5 to identify key features of culture scale up and infection, respectively. The metabolomics and proteomics datasets were log transformed prior to this analysis, and the transcriptomics data were normalized to transcripts per million (TPM) values. The proteomic and transcriptomic datasets were further filtered via the nearZeroVar function from the caret R package (version 7.0- 1), with a unique cutoff of 20 for the proteomics dataset and selecting transcripts with variances of greater than or equal to 200 were selected. In the DIABLO design matrix, we prioritized correlations between the three omics datasets by choosing a 0.6 weighted model. The features from latent component 1, from the Day 0 and Day 1 comparison and from the Day 4 and Day 5 comparison were then compiled for comparison across all four days via the R package pheatmap (version). The values were scaled and centered prior to plotting, and both rows and columns were clustered via Euclidean distance.

For the correlation analysis, genes and proteins were filtered for members that are expressed in at least 50% of samples, and at least 2/3 of replicates. Then samples were percentile normalized, and averaged across replicates. Following this, a pairwise Pearson correlation was conducted, and the results were visualized in a heat map.

For the protein-protein interaction networks, STRING (https://string-db.org/) was used to construct protein-protein interaction (PPI) networks. For the scale-up stress (D0-D1) and the amoeboaphelid stress (D4-D5), changing genes and proteins were combined into one dataset. As there are no annotations on STRING for *Monoraphidium minutum*, we used the *Chlamydomonas reinhardtii* annotation to find the closest match, and submitted those matches to STRING to generate PPI networks. The colorimetric

351 indication of the nature of each protein-protein interaction is being explained in details at https://string-
352 db.org/.

353 Based on the scant ontology analysis of *Monoraphidium minutum* and based on a recent paper [39] stating
354 that GPT4 is well-suited to ontology analysis, we prompted GPT4 as follows to identify cohesive pathways
355 from gene descriptions: "Given the gene functions from this prompt and the previous one, give me a list
356 of plausible, cohesive pathways that are being regulated in a green algae *(Monoraphidium minutum*).
357 Highlight the similarities and differences in the pathways that are engaged in the two lists." We also
358 independently verified claims with references, knowing that GPT4 and other LLMs are known to
359 hallucinate references.

360

361 **3. Results**

362

363 *3.1 Phenotypic and conditional measurements reveal distinct acclimation, growth and infection dynamics*
364 *in algae in open pond systems*

365

366 We performed a longitudinal analysis of algal growth in two 1000 L open raceway ponds, and introduced
367 an amoeboaphelid pathogen on day 4 of the experiment, tracking a total of 12 variables. Phenotypic
368 measurements included cell count, AFDW, chlorophyll concentration, total carbohydrate content, total
369 H3 histone concentration, cell size, and caspase activity (Additional File 1). In addition, we measured five
370 environmental variables within the ponds, including %DO, pH, conductivity, temperature, and light
371 intensity.

372 Across the time-course, we observed 3 growth phases of interest (color-coded in Fig. 2A):

373 a) The acclimation or lag phase (cyan). This phase occurred immediately after the inoculation in
374 the open system with refreshed nutrients. This period lasted 2 days, and growth during this phase
375 was slower than that during the other phases.

376 b). The log phase (yellow). The cells were fully acclimated to the open-pond conditions and grown
377 exponentially. This phase lasted for 4 days before the dilution and the infection and 3 days after
378 dilution.

379 c) Crash phase (brown). This phase is caused by algal death, which leads to the complete overtake
380 of the ponds by the pathogen and other opportunistic species.

381

382 The ponds behave largely similarly, although we do observe a divergence of phenotypes at later stages of
383 infection, as documented in Fig. 2.

384 To understand whether stress conditions trigger programmed cell death, we measured caspase activity
385 throughout the experiment. Caspases are proteases that catalyze the breakdown of proteins during
386 programmed cell death [40]. We observed that caspase activity initially increased after pond inoculation
387 and then gradually decreased as the cells acclimated to their new environment (Additional File. 2).

Notably, we did not observe an increase in caspase activity after infection with amoeboaphelid, suggesting that the reduction in the algal cell count could be attributed to alternative mechanisms, perhaps uncoupled from programmed cell death. To identify a specific pathway responsible, more molecular studies focused on underlying mechanism by which cells become depleted are needed. [41, 42]

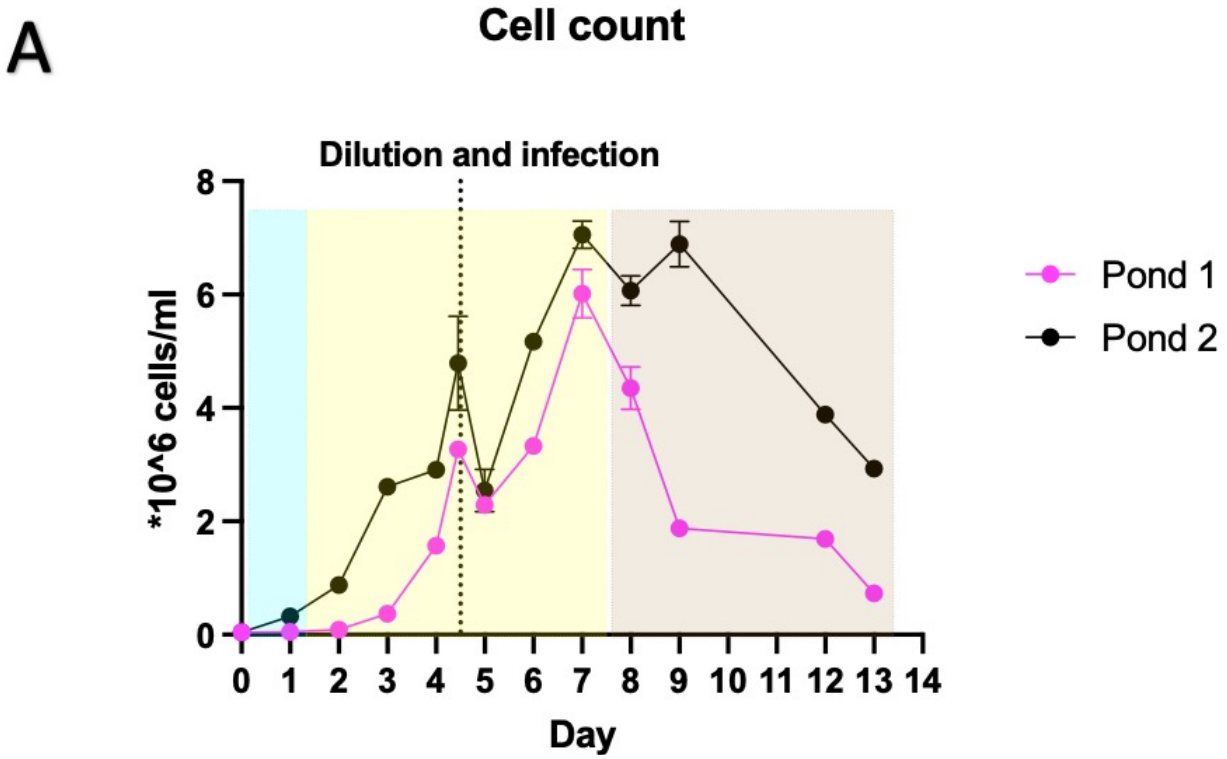

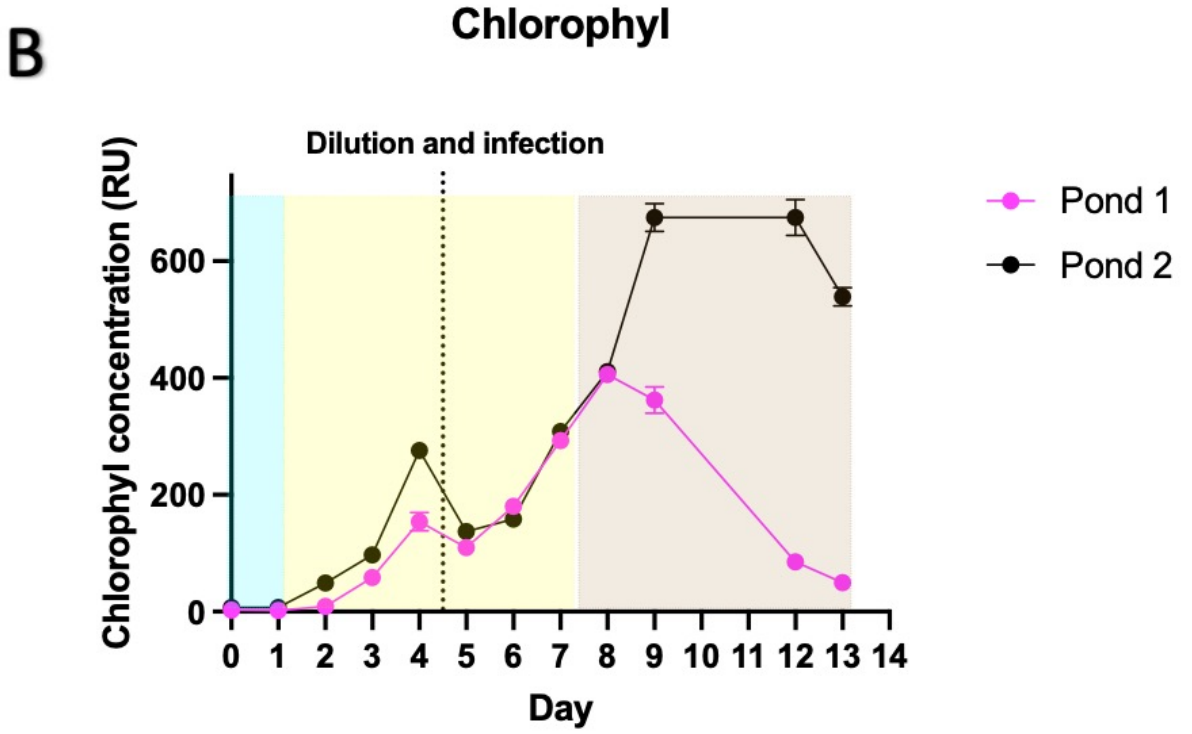

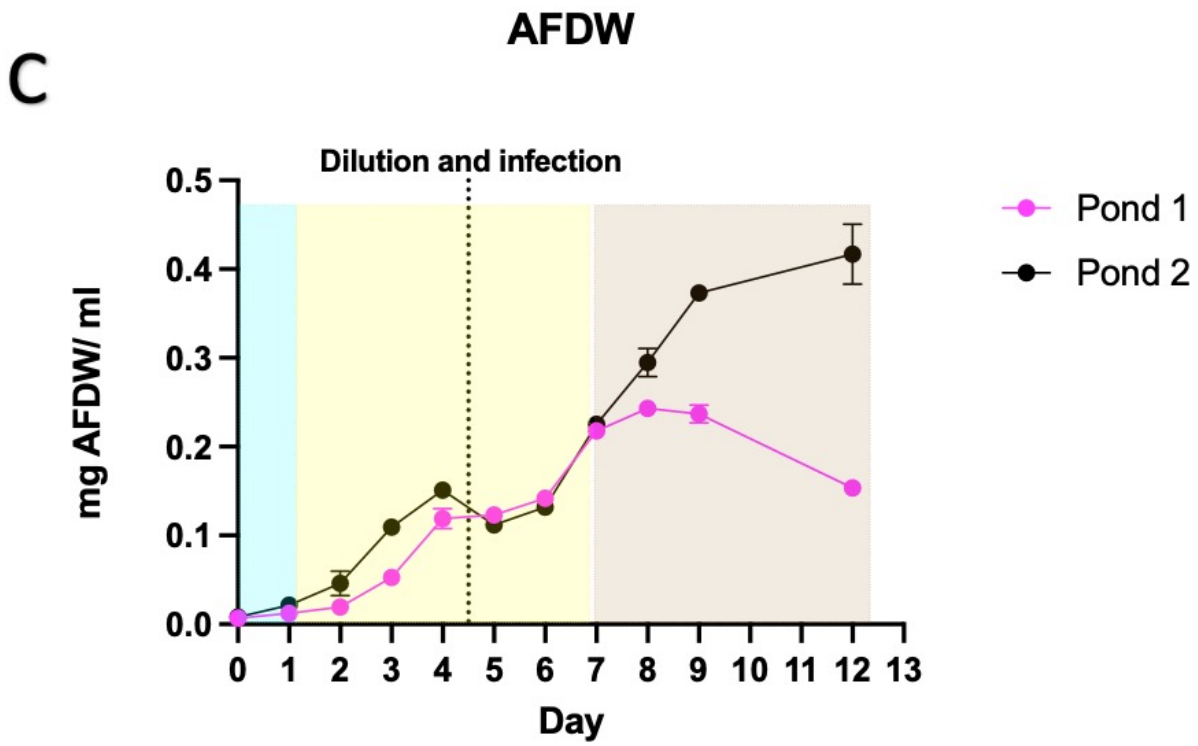

Fig. 2: Growth tracking of the M. minutum pond cultures. *A) The cell count between the three ponds. B) Chlorophyl concentration in relative units (RU) from florescence measurements. C) The Ash-free dry weight (AFDW) of algae cells in mg per mL of culture.*

For an integrated view of the phenotypic and conditional profile of the longitudinal experiment, principal component analysis (PCA) was performed with the 12 phenotypic and environmental variables. Dimension 1 represented 49.4% of the explained variance (Fig. 3A) and separated the variables that are indicative of growth, from those indicative of stress. This provides insight into the competing pressures that the algae face during cultivation, and the contributions of these pressures to outcomes.

We observe that the three distinct phases (acclimation, log, and crash) are resolved away from each other in the PCA biplot shown in Figure 3B, and we can discern a trajectory in PC space as the longitudinal experiment progresses, which is shown by connecting temporally adjacent points. While the largest adjacent transition occurred during scale-up (Day 0 to Day 1), we also observed a significant shift upon infection into a distinct PC space highlighted in brown in Figure 3B. This visualization further emphasizes the distinction between the conditions and outcomes during these phases and suggests the presence of distinct molecular profiles within the algae that likely precede outcomes. To this end, we performed transcriptomic, proteomic and metabolomic analyses across the first 6 days of this experiment.

A

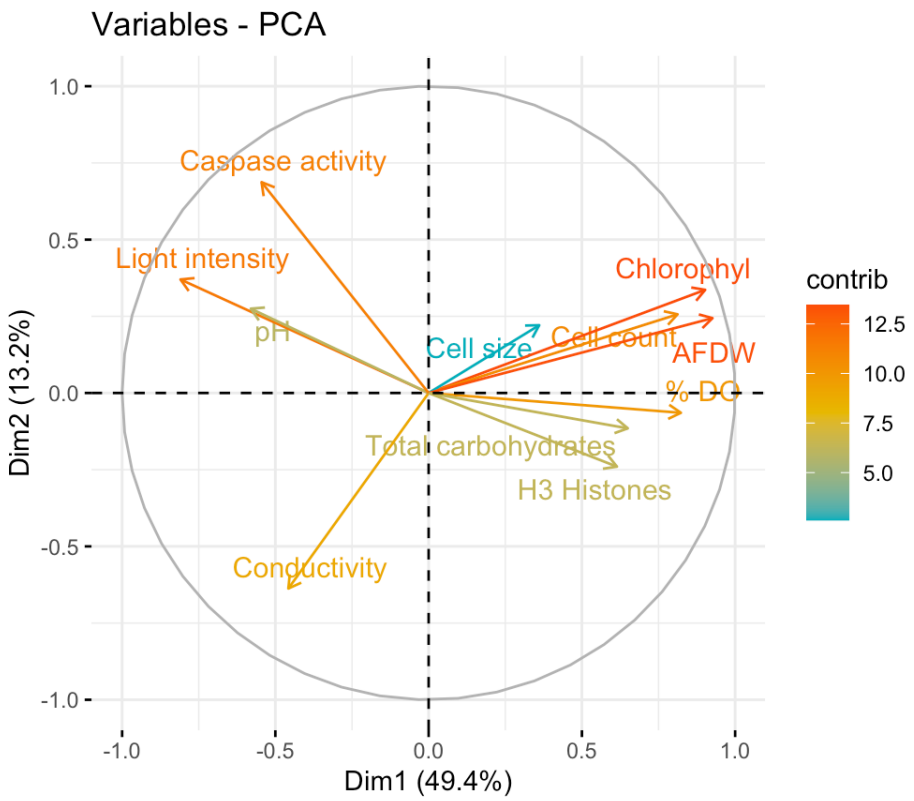
Variables - PCA
Caspase activity
Light intensity
pH
Cell size
Cell count
Chlorophyl
AFDW
%-DC
Total carbohydrates
H3 Histones
Conductivity
contrib
12.5
10.0
7.5
5.0
Dim1 (49.4%)
Dim2 (13.2%)
1.0
0.5
0.0
-0.5
-1.0

413

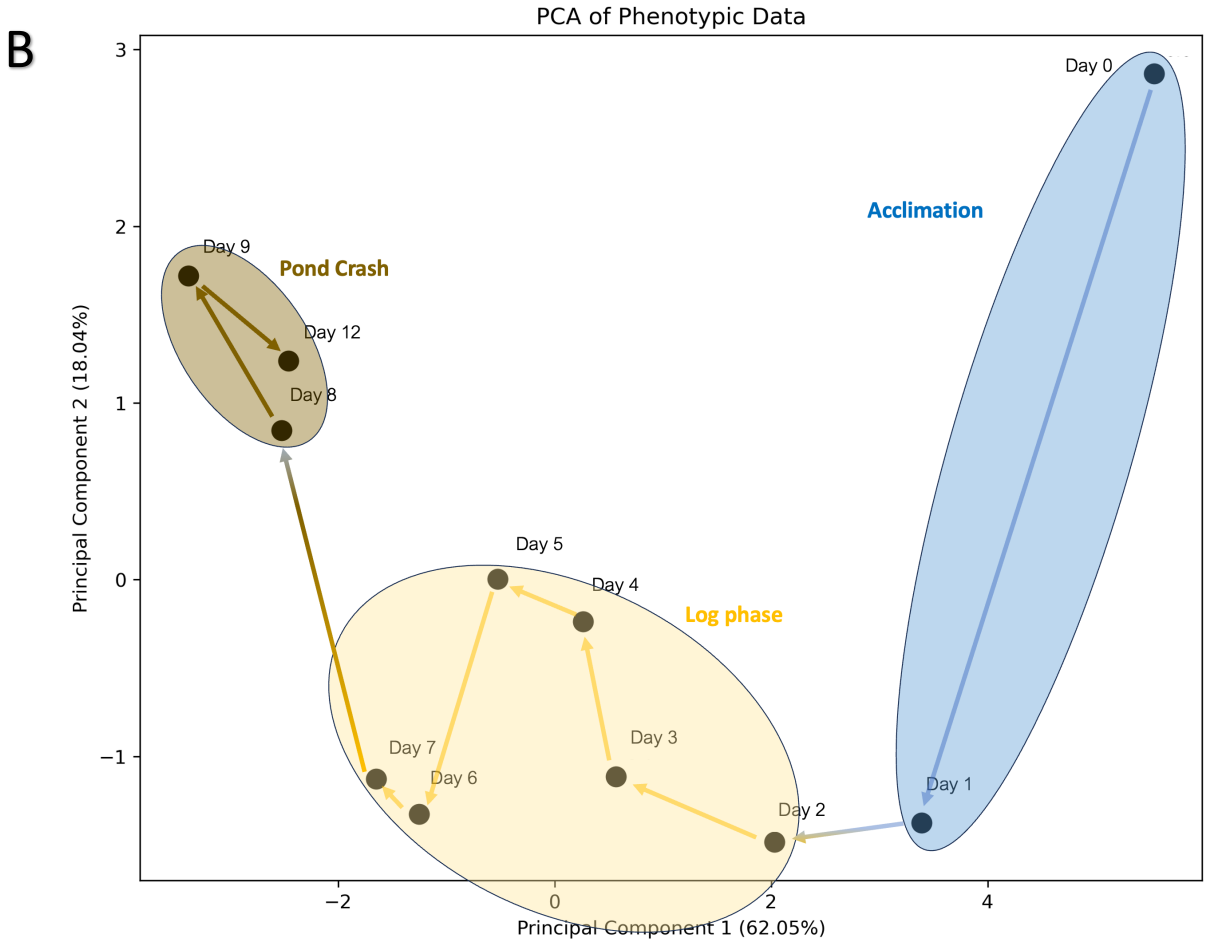

Fig. 3: PCA for 12 variables as measured at the two ponds. *A) PCA for the 12 variables used. The color of each line represents the contribution of each variable to the principal axes. Created with factoextra in R. B) Each day of the cultivation, plotted as individuals. The arrows are indicating the trajectory of each day during the culture run.*

Community composition analysis though 16/18S was also performed in order to determine the eukaryotic and bacterial composition of the ponds throughout the culture run (Fig. 4, Additional File 2). Those systems are open and expected to contain a wide variety of organisms growing in them other that *M.minutum* and the pathogen we introduced. The bacterial composition (Fig.4A), possibly consisting of both environmental and algae-associated bacteria, seems relatively stable throughout the run, with the exception of day 19, which goes beyond the total crash of the cultures. From the eukaryotic composition (Fig.4B) we can verify that, while *M. minutum* is predominant in the ponds throughout the duration of the experiment, as expected, other green algal species were co-present in relatively far smaller proportions. Notably, the pathogen was first detected on day 12, despite the fact that the culture was impacted by its presence much earlier, showing that alternative biomarkers are required for early detection of infection.

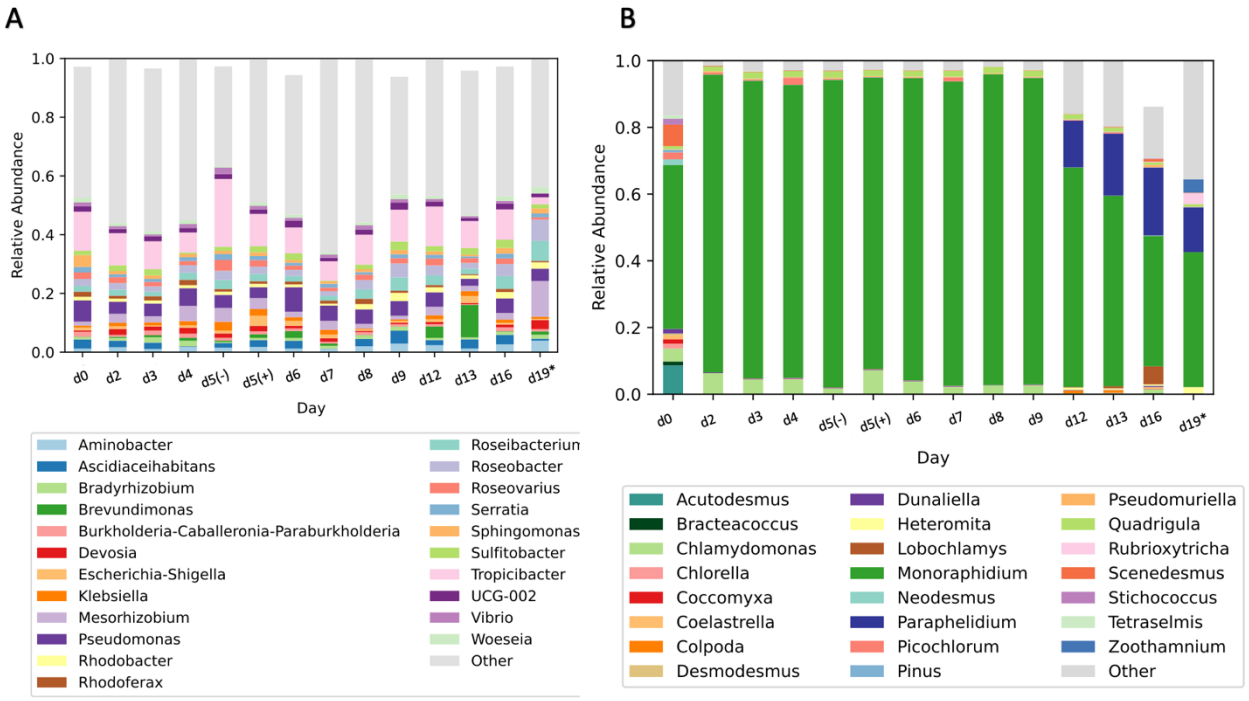

Fig.4: Microbial community composition of the ponds throughout the run until after the complete pond crashes. *A) Bacterial genera. B) Eukaryotic genera.*

3.2 Transcriptomic stability tracks with optimal growth and culture resiliency

With the goal of identifying molecular patterns within the algae that precede the observed phenotypic outcomes, we performed transcriptomic analysis from Day 0 to Day 6 (Additional File 3). The samples thus represented the acclimation period (day 0 and day 1), the preinfection log phase (day 2- day 4) and the early infection days (days 5 and 6). Throughout this period the culture is in continuous log phase and while we acknowledge that the growth and density can have an impact on the molecular state of the algae, we perform the infection prior to the slow-down and plateau phase to mitigate these effects.). For the scale-up, part of the stressor is the new density the algae are faced with, so we do not specifically adjust for this. A considerable percentage of transcripts (12.3%) were significantly differentially expressed from day 0 (the inoculation day) to day 1, reflecting the transcriptional acclimation to the scale transition from the 20 L carboys to the open 1000 L ponds (Fig.5A). This difference in expression was multiple times greater than any daily difference observed during the following days. This included days after infection where only 0.7% of the transcripts were significantly differentially expressed. Consistent with the algae being in a homeostatic growth phase, we saw very few differences in gene expression across non-stressor days, suggesting that the majority of changes occur as a result of stress rather than growth.

We performed PCA on the transcriptomic data to determine whether the longitudinal trajectory was comparable to that of our phenotypic and environmental variables (Fig. 5B and 5C). The transition from Day 0 to Day 1 was the most striking, reflecting the rapid and large transcriptomic response to the 1000 L pond conditions. The distributions of the days corresponding to the pre-infection log phase, on the other hand, are closer in PC space, reflecting transcriptional stability during that growing stage. A clear

455 distinction between the distribution of the preinfection and postinfection days was also observed, as a
456 result of both the culture dilution and the introduction of the pathogen. In fact, unlike in Fig. 3B where
457 the measured environmental and phenotypic variables postinfection were in a distinct cluster away from
458 the scale-up, the early postinfection transcriptomic profile trends back toward the acclimation phase
459 profile but still remains distinct from them.

460

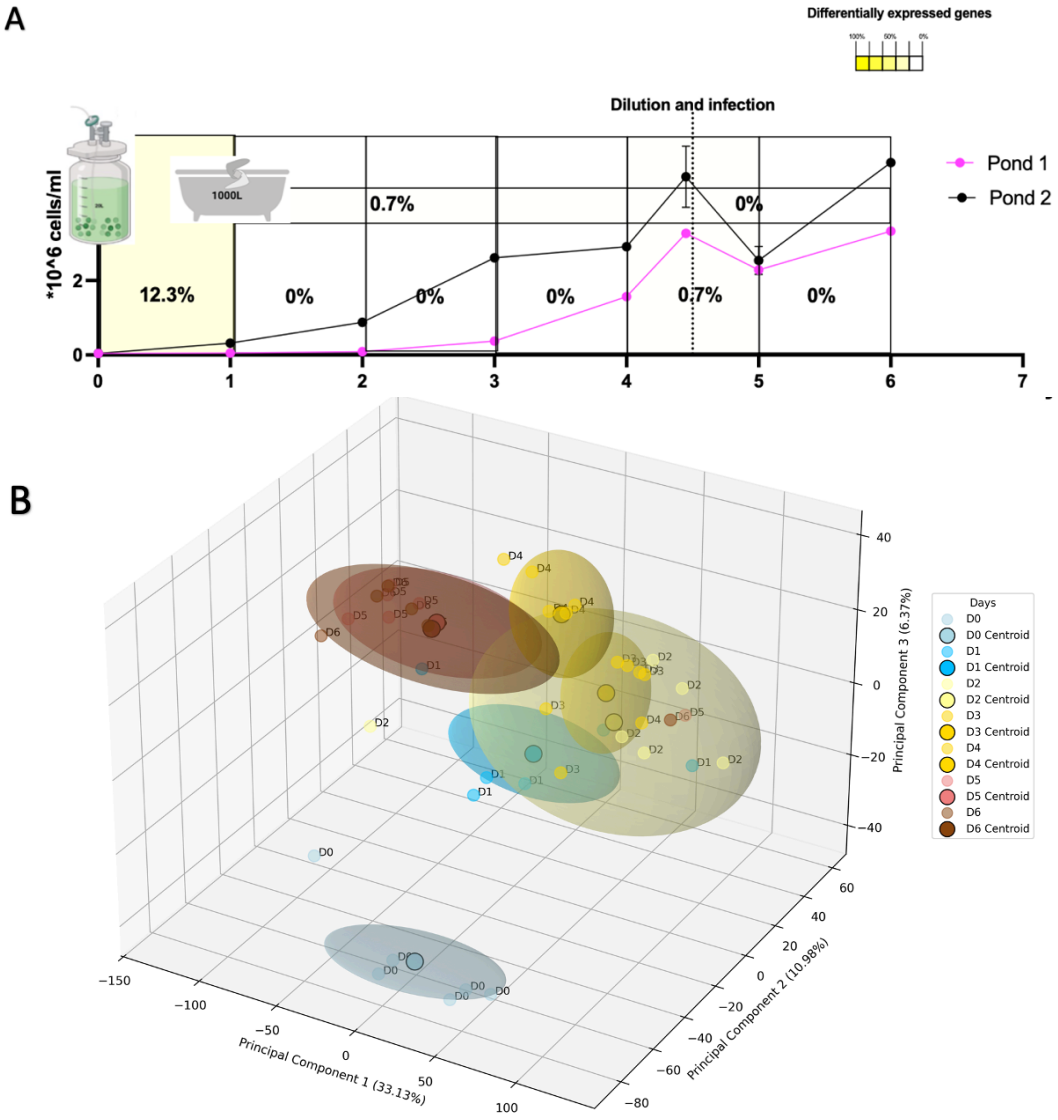

461

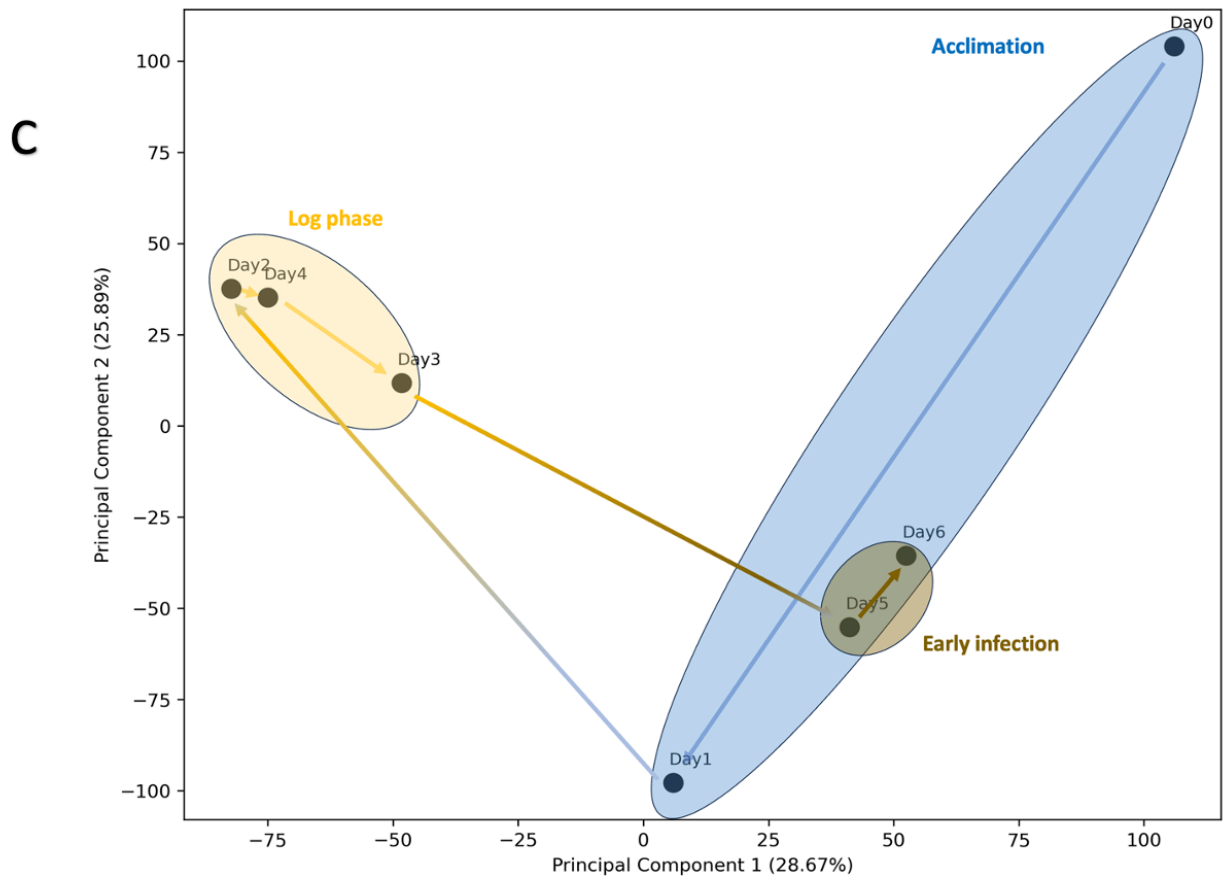

Fig. 5: Comparative analysis of the transcript abundances overlaid with cell growth results. *A) Growth curve of both ponds over the time course, with transcriptomic data collected on the same day as growth was measured (as shown by points on the curve). Percentages of differentially expressed genes between specific daily points within the cultivation are shown by the numbers. B) 3D PCA analysis of the transcriptomics, showing the distribution of all the technical replicates for each day from the two ponds. Centroids are indicated with a darker point, and standard deviation is indicated by the shaded circle. C) 2D representation of the PCA showing the average points for each day. The arrows indicate the trajectory of the time course.*

The annotation of *M. minutum* genome is incomplete, making traditional pathway analysis complicated. To further investigate the regulation behind those transcriptional changes we performed a motif analysis among the promoter regions of the genes that were significantly differentially expressed to identify regions that could be bound by conserved transcription factors. We focused on the transitions between day 0 and day 1 (Table 1), and between day 4 and day 5 (Table 2). The ten most enriched motifs that emerged from each group are shown in Table 1 and Table 2, alongside their best matches from other organisms. Most identified motifs are unique to each transition.

Table 1: Enriched promoter motifs at the scale adaptation-related genes.

	Motif	% of Targets	P- value	Best match/ Details
1		21.63%	1e-10	NCU02182/MA1434.1/Jaspar (0.811)

2	CGATCAGT	46.35%	1e-9	Initiator/Drosophila-Promoters/Homer (0.761)
3	TTGATGCC	38.02%	1e-8	ZNF549/MA1728.2/Jaspar (0.770)
4	CCGCACGGCA	47.40%	1e-8	NAC035/MA2046.2/Jaspar (0.832)
5	CCCGTATG	55.14%	1e-8	Gcm2/MA0917.1/Jaspar (0.770)
6	GGCGCCCGCTCG	32.53%	1e-7	SeqBias: CG-repeat (0.735)
7	GAATACGC	31.84%	1e-7	Tp_0225(RRM)/Thalassiosira_pseudonana-RNCMPT00225-PBM/HughesRNA (0.742)
8	CATTCCGT	39.95%	1e-7	TEC1/MA0406.2/Jaspar (0.814)
9	CCTATTTG	28.10%	1e-7	Br/MA0011.2/Jaspar (0.819)
10	ATATCAGC	20.47%	1e-7	SWI5/Literature(Harbison)/Yeast (0.770)

Table 2: Enriched promoter motifs at the infection-related genes.

	Motif	% of Targets	P- value	Best match/ Details
1	CTAGTCTC	66.67%	1e-9	ARF1(ABI3/VP1)/Arabidopsis thaliana/AthaMap (0.719)
2	CATACGGG	64.41%	1e-9	gcm2/MA0917.1/Jaspar (0.770)
3	GGCATCAA	35.59%	1e-8	Abd-B/dmmpmm(Bergman)/fly(0.775)
4	GGTCACTT	32.33%	1e-8	RTG3/Literature (Harbison)/Yeast (0.882)
5	TCTTCCGT	50.38%	1e-8	RGT1/Literature (Harbison)/Yeast (0.775)
6	GCCCCGCTGC	28.57%	1e-8	Sp1(Zf)/Promoter/Homer (0.747)
7	AGCACTTGCA	40.85%	1e-7	bHLH78/MA0963.1/Jaspar (0.804)
8	CACGTGCCTC	26.07%	1e-7	HES2/MA0616.3/Jaspar (0.840)
9	GACTGATC	23.06%	1e-7	ZmHOX2a (2) (HD-HOX)/Zea mays/AthaMap (0.795)
10	TTCAATCA	41.10%	1e-7	PBX1/MA0070.2/Jaspar (0.812)

3.3 Transcriptomic and phenotypic data reveal the light and dissolved oxygen (DO) regulation of protein translation and photosynthesis

One of the advantages of performing time-course transcriptomics on large open cultures in a poorly studied species such as *M. minutum* is that it allows for the extraction of reliable and useful information

about specific environmentally triggered expressed genes. Light intensity and DO are two environmental factors known to influence outcomes in algae. To understand their role in the outcome of our cultures, we used a program called GEMMA that applies mixed linear models to connect phenotypes with large-scale molecular data [34]. We identified transcripts whose expression was positively or negatively correlated with light intensity and %DO across samples (Figs. 6 and 7).

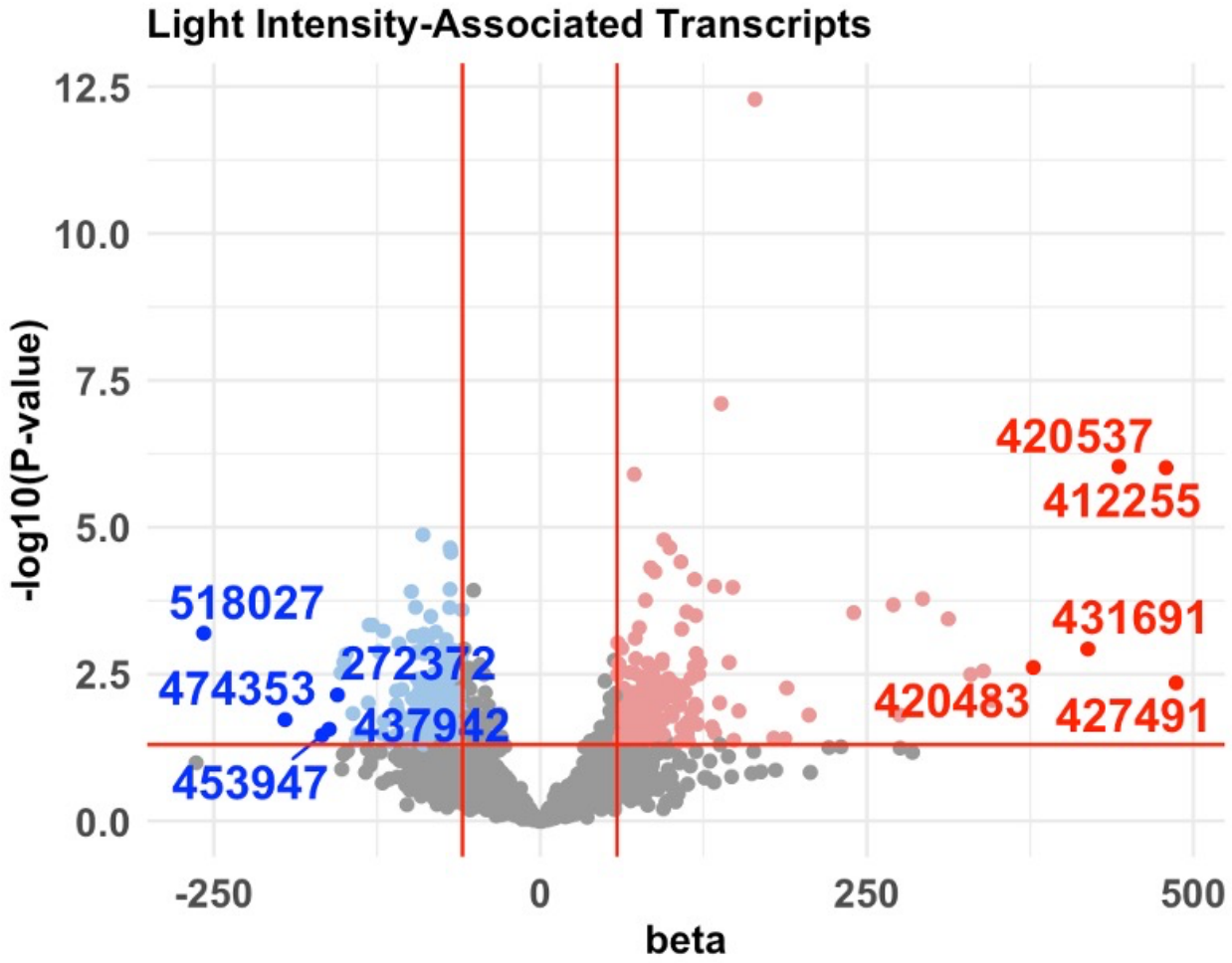

Fig. 6: GEMMA analysis, revealing the genes which are correlated with light intensity. *The volcano plot shows the significance and the extent of the correlation between the light intensity and the transcript abundance. The top 5 up- and downregulated genes by light are indicated.*

[43]To further understand the regulatory genomic elements that might contribute to light-dependent changes in gene expression, we performed a motif analysis on the promoter regions of all the genes whose expression was significantly up- or downregulated by light (Tables 5 and 6). Among the most significant motifs from the upregulated genes, two corresponded to transcription factors from two higher plant species, *Arabidopsis* and *Zea mays*.

Table 3: The annotations of the top 5 genes whose expression was upregulated with light.

JGI ID	beta	Gene product
427491	486.8095	ribosomal protein S9 component of cytosolic 80S ribosome and 40S small subunit
412255	479.0458	40S ribosomal protein S29-like
420537	442.9904	putative 40S ribosomal protein S3a
431691	419.257	Translation protein SH3-like domain-containing protein
420483	377.4611	component of cytosolic 80S ribosome and 60S large subunit

Table 4: The annotations of the top 5 genes whose expression was downregulated with light.

JGI ID	beta	Gene product
518027	-257.7188	heat shock cognate 70 kDa protein 4-like
474353	-195.5336	hypothetical protein
453947	-167.1721	eukaryotic translation initiation factor 5
437942	-161.7026	photosystem I protein P30
272372	-155.3597	hypothetical protein

Table 5: Enriched promoter motifs at the light upregulated genes.

	Motif	% of Targets	P- value	Best match/ Details
1		21.74%	1e-8	Unknown3/Arabidopsis-Promoters/Homer (0.710)
2		33.33%	1e-8	CAT8/MA0280.2/Jaspar (0.749)
3		23.91%	1e-7	ZmHOX2a (2) (HD-HOX)/Zea mays/AthaMap (0.823)
4		23.91%	1e-7	AT5G04390/MA1736.2/Jaspar (0.752)

5	TACTGTCG	23.91%	1e-7	lsy-2/MA2181.1/Jaspar (0.874)
6	GGGCCCCGCC	47.46%	1e-7	Sp1(Zf)/Promoter/Homer (0.783)
7	TCTTCCGT	30.80%	1e-6	RGT1/Literature (Harbison)/Yeast (0.793)
8	CCAATTGG	30.43%	1e-6	insv/MA2315.1/Jaspar (0.821)
9	CTGGCAGCAA	16.67%	1e-6	ZNF549/MA1728.2/Jaspar (0.779)
10	GGCGCGGCGATC	30.80%	1e-5	ZNF610/MA1713.2/Jaspar (0.721)

Table 6: Enriched promoter motifs at the light downregulated genes.

	Motif	% of Targets	P- value	Best match/ Details
1	CAAATCGG	36.93%	1e-10	br/MA0011.2/Jaspar (0.725)
2	TTCAATCA	41.83%	1e-9	PB0188.1_Tcf7l2_2/Jaspar (0.842)
3	GGCAGAGCCC	32.35%	1e-8	ZNF331/MA1726.2/Jaspar (0.870)
4	AGCAAGGGGG	23.53%	1e-8	MSN4(MacIsaac)/Yeast (0.777)
5	GCCCGGTGTG	27.12%	1e-7	MET31(MacIsaac)/Yeast (0.683)
6	AGTGCCTA	26.47%	1e-7	PHD1(MacIsaac)/Yeast (0.856)
7	CCTTATAT	17.97%	1e-6	PUF68(RRM)/Drosophila_melanogaster-RNCMPT00141-PBM/HughesRNA (0.805)
8	GATCACTC	27.45%	1e-6	ZmHOX2a(2)(HD-HOX)/Zea mays/AthaMap (0.799)
9	TTGACCGCGC	17.32%	1e-6	WRKY1/MA0589.2/Jaspar (0.869)
10	ACGGAATG	41.50%	1e-6	TEAD2/MA1121.2/Jaspar (0.808)

A similar GEMMA analysis was repeated with the genes most correlated with %DO. Among the ten most upregulated and downregulated genes correlated with %DO (Fig. 7A, Tables 7 and 8), multiple genes related to photosynthesis and carbon fixation were identified. A phosphoribulokinase/uridine kinase, an enzyme responsible for a key step in the Calvin-Benson cycle, a light-harvesting protein of Photosystem I, and a protein involved in programmed cell death were among the most upregulated genes correlated with DO. We performed motif analysis on the promoter regions of all the genes correlated with DO (Tables 9 and 10). We observed enrichment of the binding site for the same transcription factor from the diatom *Thalassiosira pseudonana* at both the up- and downregulated genes from the DO.

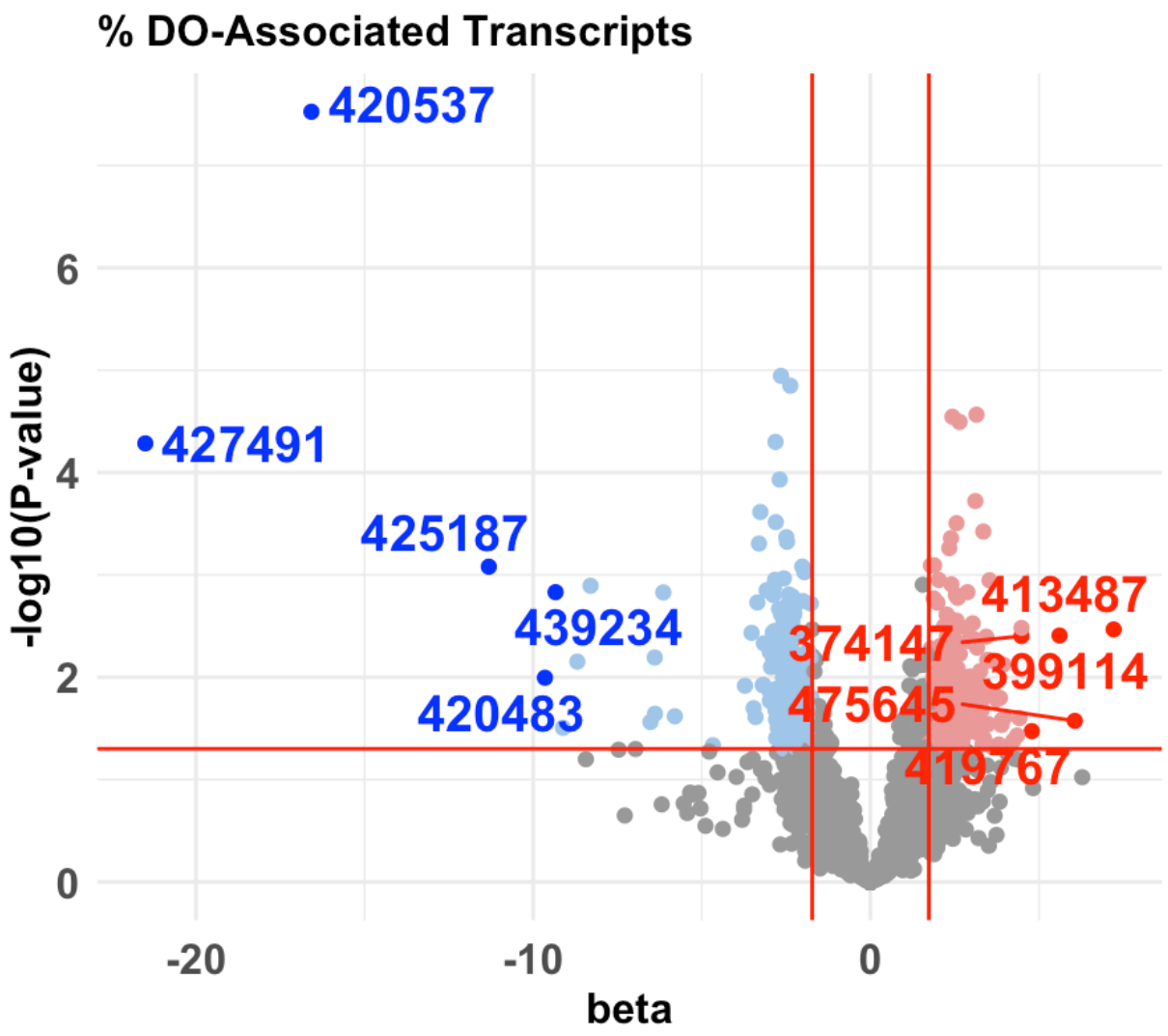

Fig. 7: GEMMA analysis, revealing genes correlated with %DO. *The volcano plot shows the significance and the extent of the correlation between the light intensity and the transcript abundance. The top 5 up- and downregulated genes by %DO are indicated.*

Table 7: The annotations of the top 5 genes whose expression was upregulated with %DO.

JGI ID	beta	Gene product
413487	7.216919	Phosphoribulokinase / Uridine kinase family-domain containing protein
475645	6.064846	hypothetical protein
399114	5.610648	expressed protein

419767	4.78923	light-harvesting chlorophyll-a/b protein of photosystem I
374147	4.481988	Programmed cell death protein 2, C-terminal putative domain-domain containing protein

525

526 *Table 8: The annotations of the top 5 genes whose expression was downregulated with %DO.*

JGI ID	beta	Gene product
427491	-21.50261	ribosomal protein S9 component of cytosolic 80S ribosome and 40S small subunit
420537	-16.57716	putative 40S ribosomal protein S3a
425187	-11.31527	ribosomal protein L3 component of cytosolic 80S ribosome and 60S large subunit
420483	-9.651194	component of cytosolic 80S ribosome and 60S large subunit
439234	-9.335318	P-loop containing nucleoside triphosphate hydrolase protein

527

528 *Table 9: Enriched promoter motifs at the %DO upregulated genes.*

	Motif	% of Targets	P- value	Best match/ Details
1		23.02%	1e-8	GATA15(C2C2gata)/col-GATA15-DAP-Seq (GSE60143)/Homer (0.833)
2		28.68%	1e-8	ARR1/Literature (Harbison)/Yeast (0.743)
3		41.51%	1e-7	NKX2-3/MA0672.2/Jaspar (0.771)
4		21.89%	1e-6	ABF2/MA0266.2/Jaspar (0.803)
5		37.74%	1e-6	ZNF549/MA1728.2/Jaspar (0.751)
6		38.87%	1e-6	Tp_0225(RRM)/Thalassiosira_pseudonana-RNCMPT00225-PBM/HughesRNA (0.796)
7		57.36%	1e-6	ZNF415(Zf)/HEK293-ZNF415.GFP-ChIP-Seq (GSE58341)/Homer (0.760)
8		17.74%	1e-6	Vdr/MA0693.4/Jaspar (0.846)
9		16.98%	1e-6	EFL-1(E2F)/cElegans-L1-EFL1-ChIP-Seq(modEncode)/Homer (0.719)
10		28.30%	1e-6	REB1/SacCer-Promoters/Homer (0.815)

Table 10: Enriched promoter motifs at the %DO downregulated genes.

	Motif	% of Targets	P- value	Best match/ Details
1		43.38%	1e-12	PB0188.1_Tcf7l2_2/Jaspar (0.841)
2		40.40%	1e-9	Tp_0225(RRM)/Thalassiosira_pseudonana-RNCMPT00225-PBM/HughesRNA (0.730)
3		25.17%	1e-9	RTG3/Literature (Harbison)/Yeast (0.896)
4		32.78%	1e-8	ABF2/MA0266.2/Jaspar (0.781)
5		41.72%	1e-8	ZNF549/MA1728.2/Jaspar (0.753)
6		27.48%	1e-8	STB4/STB4_YPD/ [] (Harbison)/Yeast (0.723)
7		34.44%	1e-8	Syncrip (RRM)/Xenopus_tropicalis-RNCMPT00281-PBM/HughesRNA (0.754)
8		21.85%	1e-7	ZBED4/MA2328.1/Jaspar (0.742)
9		18.54%	1e-7	RAP211 (AP2EREBP)/colamp-RAP211-DAP-Seq (GSE60143)/Homer (0.722)
10		34.44%	1e-7	ZNF415(Zf)/HEK293-ZNF415.GFP-ChIP-Seq (GSE58341)/Homer (0.721)

3.4 Proteome composition shifts during algal growth and stress response.

To gain additional molecular information from the algae as they sensed transitions in their environment, a comprehensive proteomic analysis was conducted on the two pond populations longitudinally. Similar to the transcriptomics data, PCA of the proteomics data (Additional File 4) revealed a highly dynamic phase during the first two days of the culture (Fig. 8). After entering the log phase, however, the proteome becomes progressively more stable, while at the same time maintaining a distinct profile between the pre- and postinfection periods. This was in contrast to the more dynamic changes in the transcriptome after infection, highlighted in the plasticity of the transcriptional regulation in relation to the environmental triggers in comparison with the stability of the protein expression. Further analysis of the correlations between specific transcripts and proteins will be discussed later in this article.

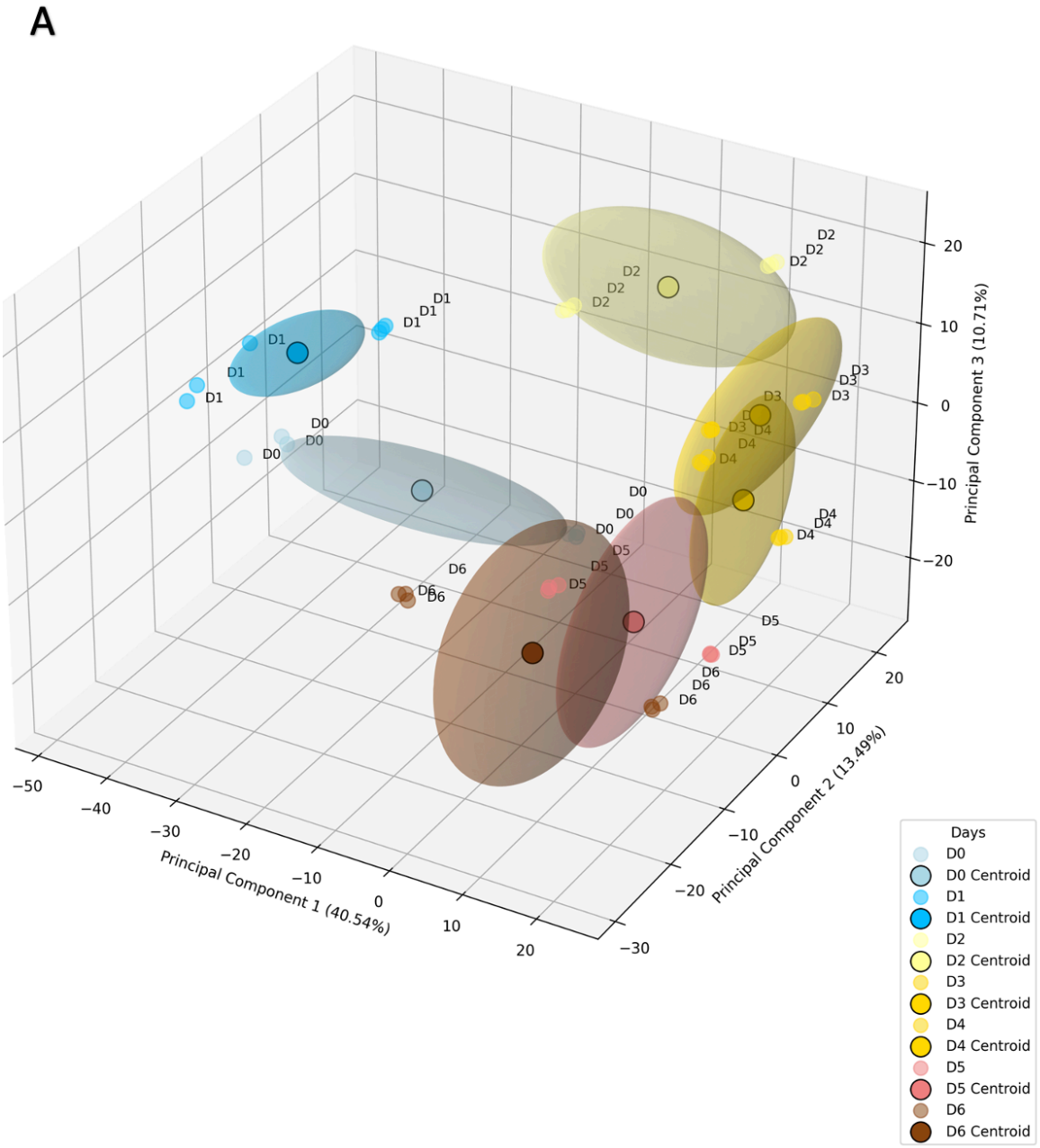
A
Principal Component 1 (40.54%)
Principal Component 2 (13.49%)
Principal Component 3 (10.71%)
Days
D0
D0 Centroid
D1
D1 Centroid
D2
D2 Centroid
D3
D3 Centroid
D4
D4 Centroid
D5
D5 Centroid
D6
D6 Centroid

543

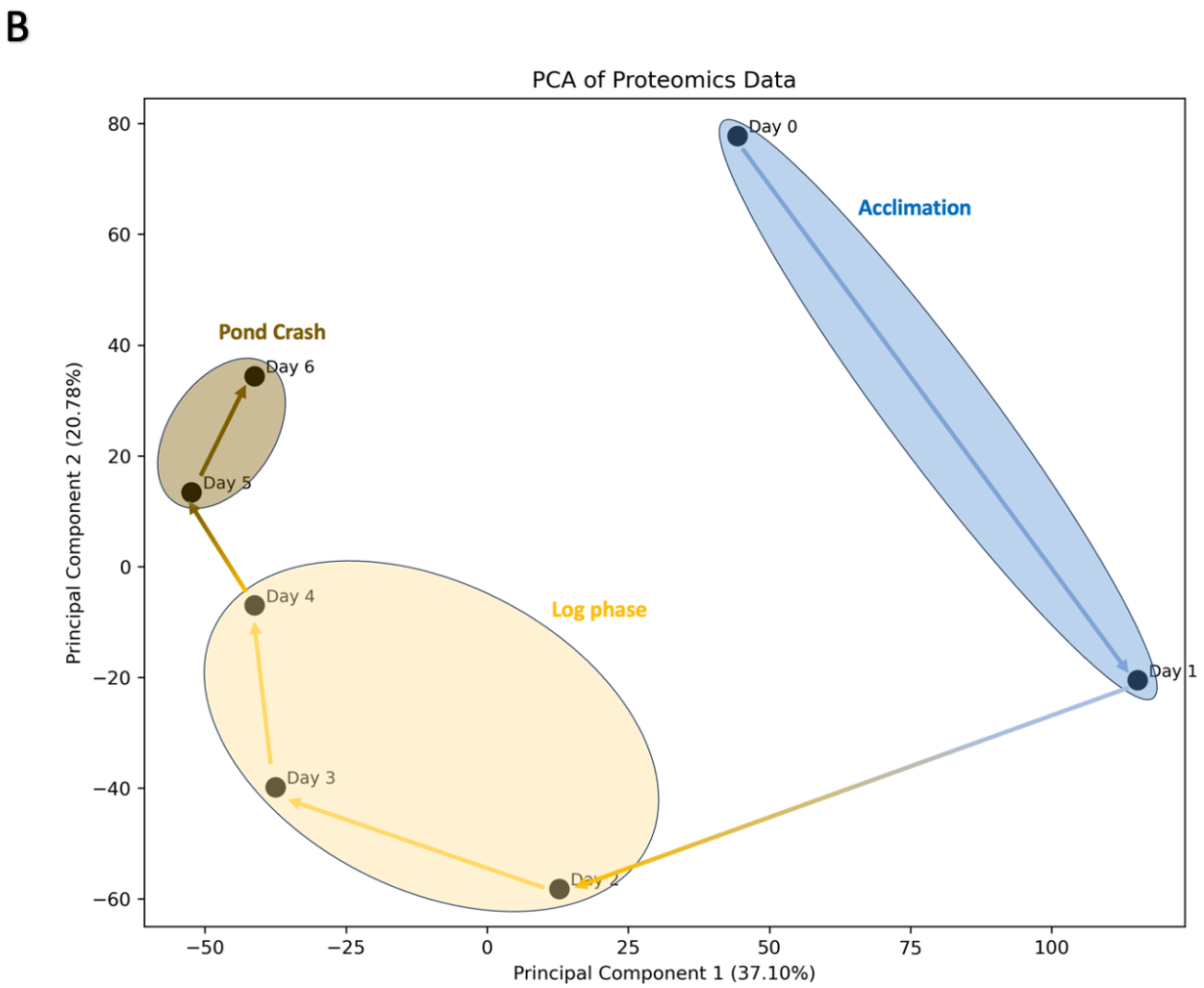

Fig. 8: PCA of the proteomics. *A) 3D PCA analysis of the proteomics, showing the distribution of all the technical replicates for each day from the two ponds. Centroids are indicated with a darker point, and standard deviation is indicated by the shaded circle. B) 2D representation of the PCA showing the average points for each day. The arrows indicate the trajectory of the time course.*

3.5 Metabolomic analysis reveals potential indicators of the stress response and pathogen infection.

PCA of the metabolites (Additional File 5) revealed distinct profiles during the three phases of cultivation similar to the transcriptomic and proteomic PCAs (Fig. 9A and 9B). Interestingly, day 3, which is in the middle of the log phase, stood out in the PCA. This contrasted with the observation made from transcriptomics. While log phase was linked with transcriptomic stability, the metabolic profile is very dynamic during the growth phase.

We performed clustering analysis of the longitudinal metabolomics data to further understand the metabolites that covaried (Fig. 9C). We used DPGP [44], a nonparametric clustering algorithm that can factor in longitudinal information, to separate metabolites into clusters on the basis of their patterns in abundance. We found that many metabolites either had their peak or trough on days 3 or 4, the midpoint

of the log phase (clusters 2, 4, 6 and 8 and 9). The most abundant cluster (Cluster 1) included metabolites whose abundance steadily increased over time. On the other hand, Cluster 5 showed the opposite trend, starting with high abundance and slowly decreasing in abundance over time.

Hierarchical clustering of the scaled and centered metabolite abundances in the heatmap, shown in Fig. 9D, highlights the emergence of three groupings of metabolites, and is in relative accordance with the DPGP clustering. The first group consists of the metabolites whose abundance peaks in the lag phase. The second group peaked in the log phase. The last group, which was the largest by number, contained the metabolites that reached their peak abundance after the infection. The last group included hormones and steroids, such as 5-Dihydrotestosterone, 7-Hydroxytestosterone, Estrone, Estriol and 19-Norandrostenedion.

A

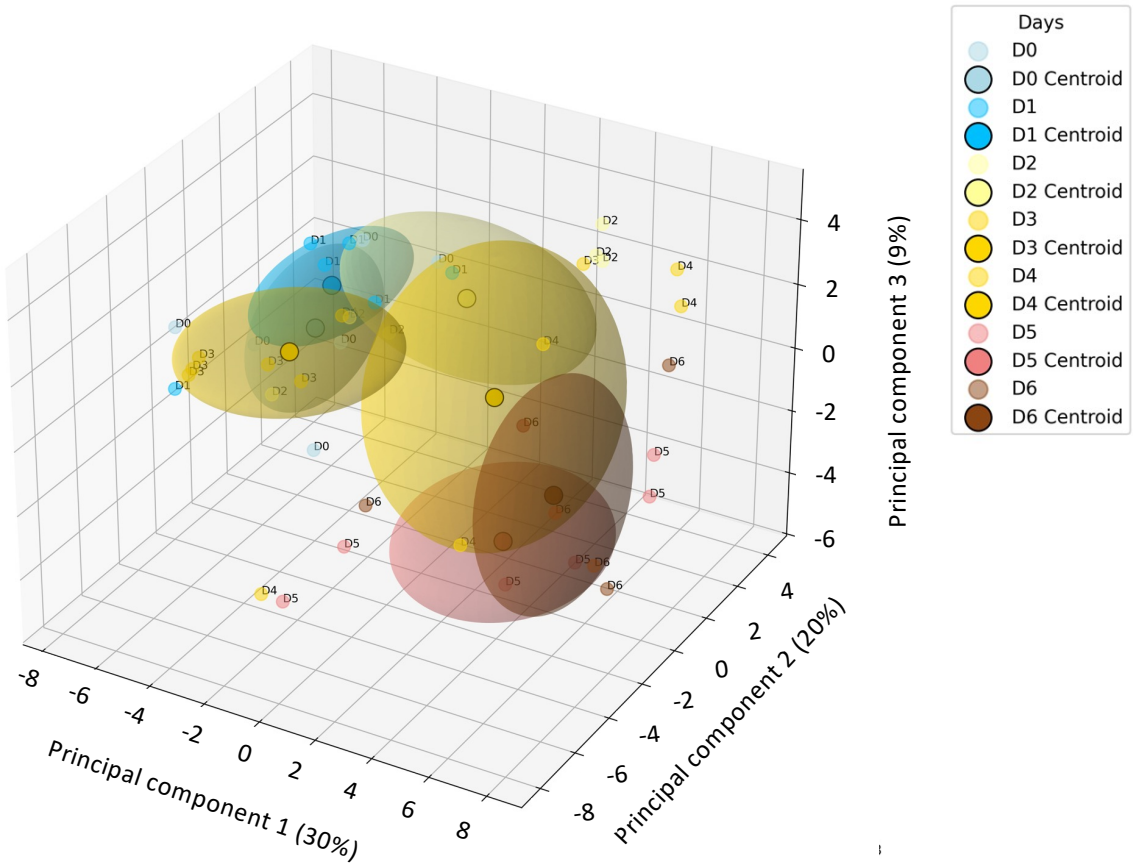

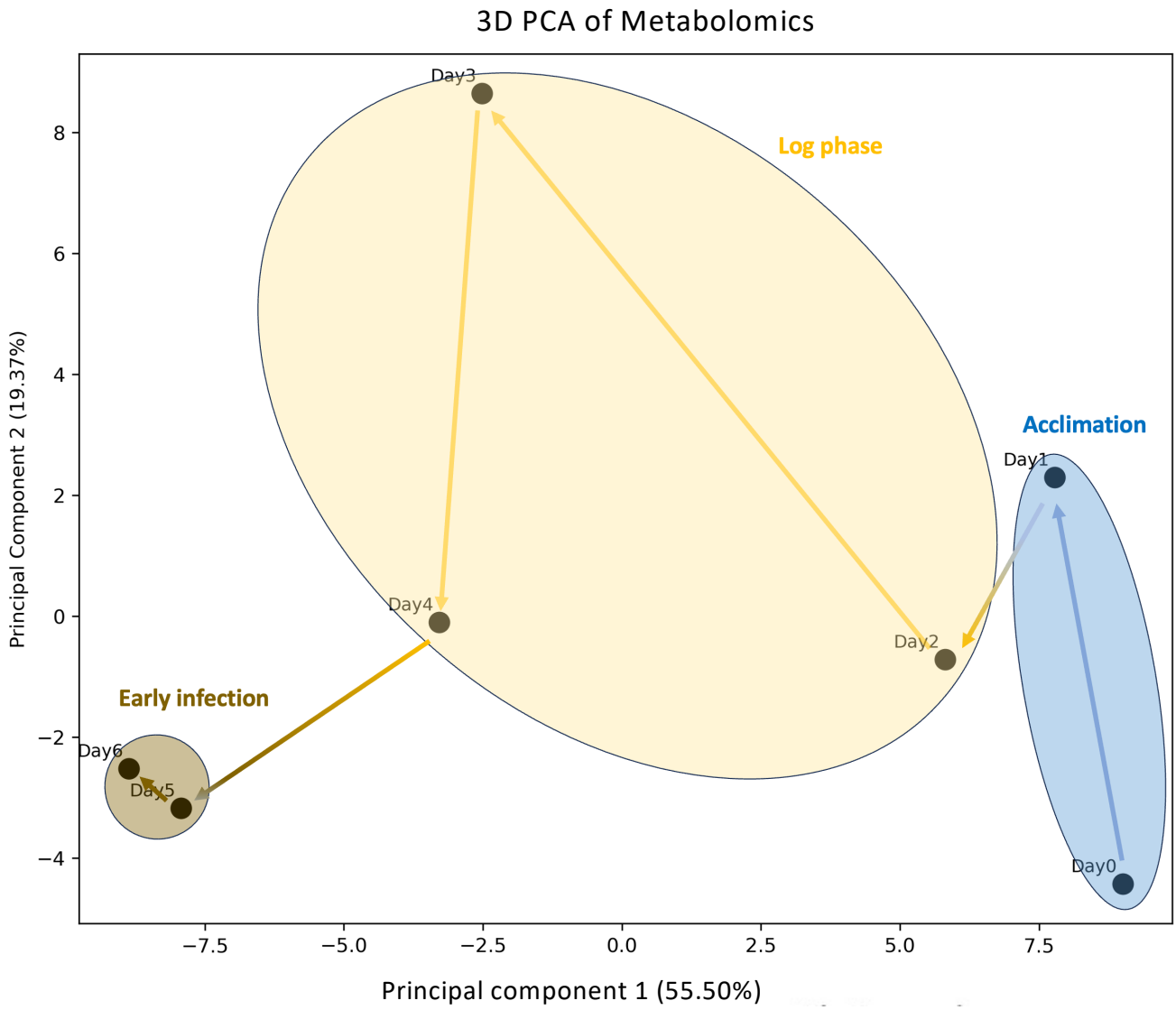
B
3D PCA of Metabolomics
Log phase
Acclimation
Early infection
Day0
Day1
Day2
Day3
Day4
Day5
Day6
Principal Component 2 (19.37%)
Principal component 1 (55.50%)
8
6
4
2
0
−2
−4
−7.5
−5.0
−2.5
0.0
2.5
5.0
7.5

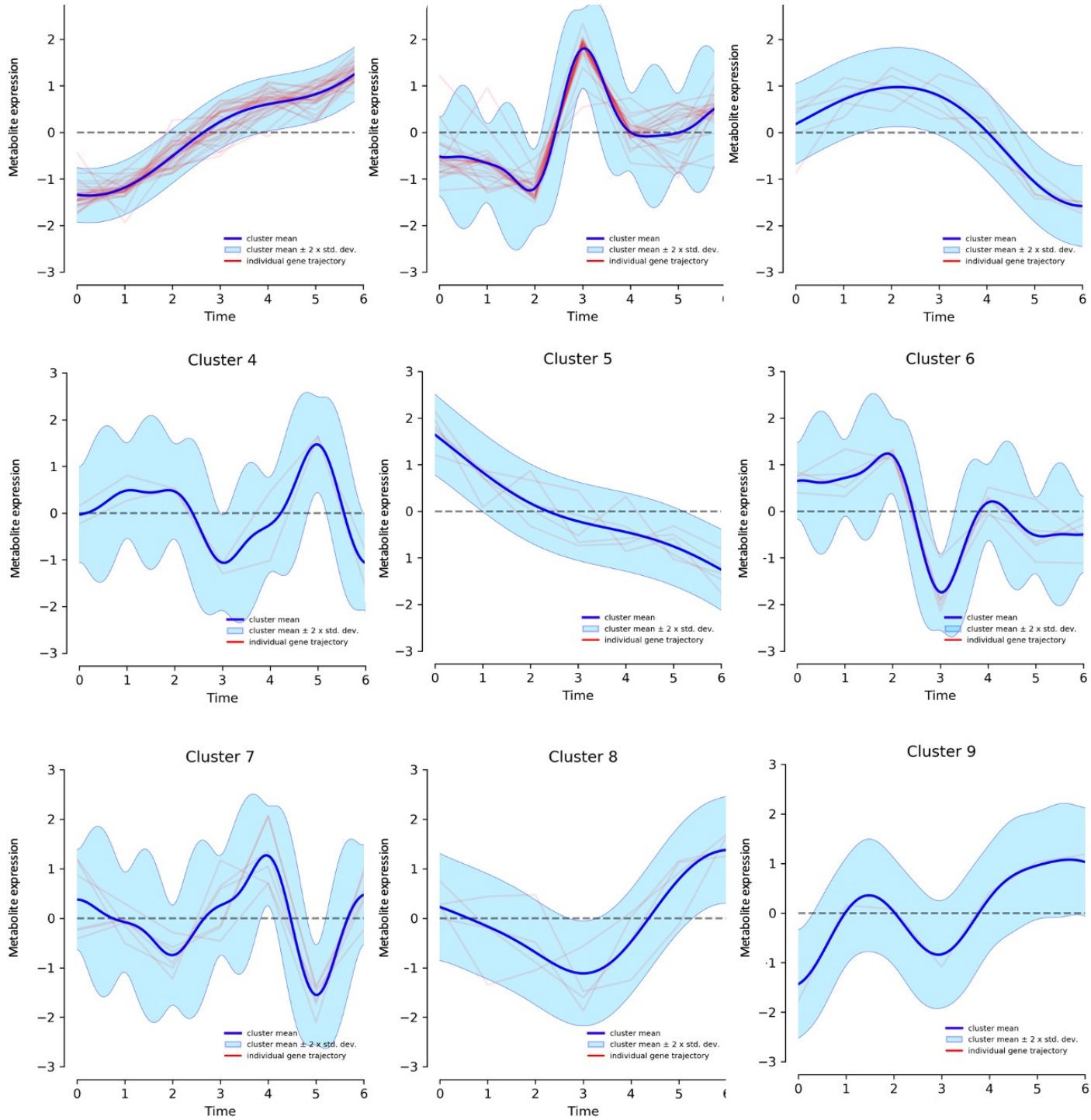
Cluster 4
Cluster 5
Cluster 6
Cluster 7
Cluster 8
Cluster 9
Metabolite expression
Time
cluster mean
cluster mean ± 2 x std. dev.
individual gene trajectory

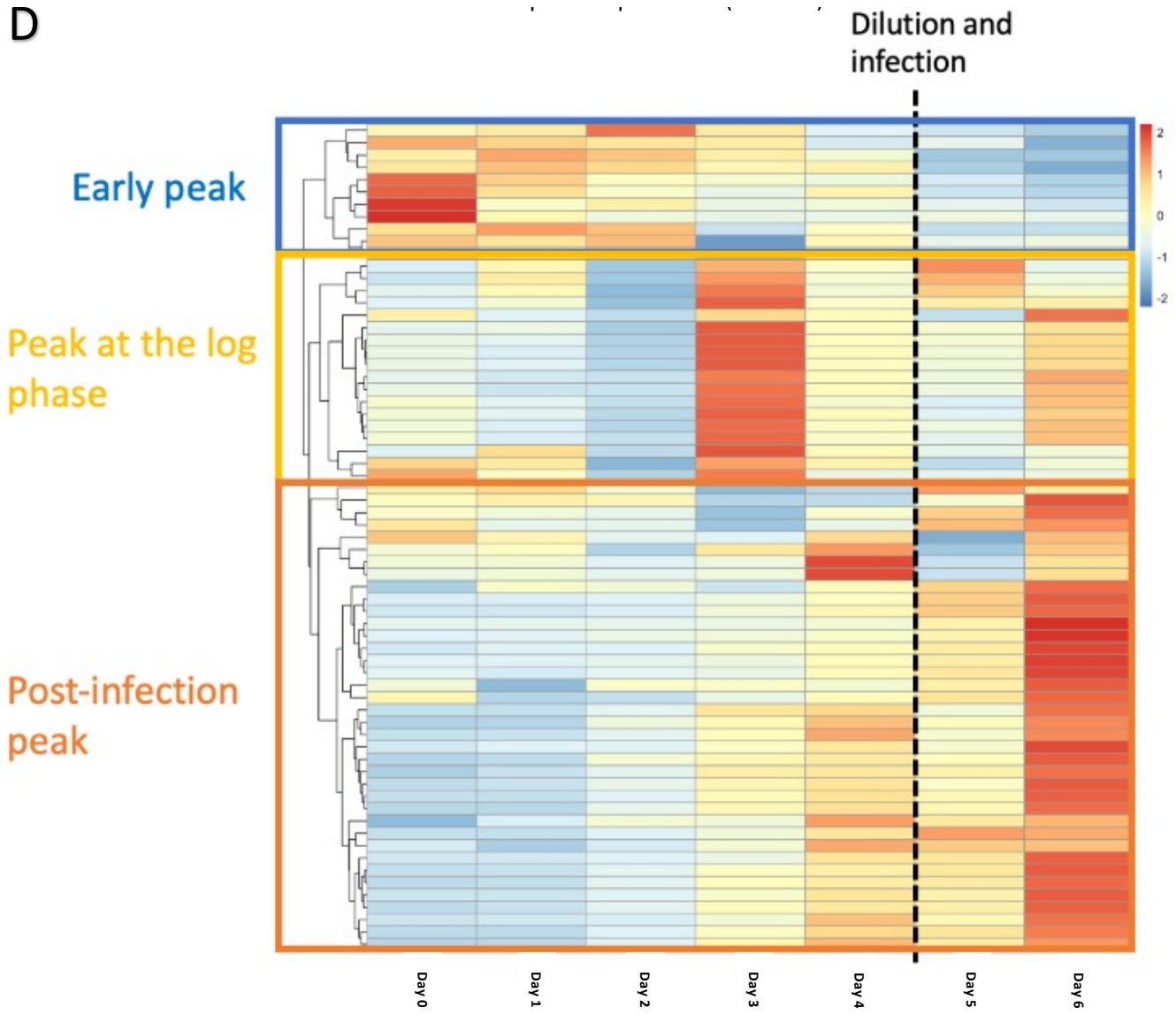

Fig. 9: The metabolomic analysis from the pond cultures. *A) 3D PCA analysis of the metabolomics, showing the distribution of all the technical replicates for each day from the two ponds. Centroids are indicated with a darker point, and standard deviation is indicated by the shaded circle. B) 2D representation of the PCA showing the average points for each day. The arrows indicate the trajectory of the time course. C) Clustering analysis of the abundance of the metabolites throughout the studied period, via DPGP. D) Heatmap with the hierarchical clustering of the significantly produced metabolites throughout the run of the cultivation. It includes the metabolites which had more that 10x higher signal than the metabolites in the blank.*

To further verify our findings from the metabolomic analysis on the ponds, specifically on the discovery of infection biomarkers, we repeated the experiment at the flask level in laboratory settings (Additional File 6). The cultures were infected with the same amoeboaphelid between day 4 and day 5 and samples for metabolomics were taken on specific days and analyzed. It should be noted here that the smal-scale experiemnt was conducted in a closed and axenic environment, unlike the large-scale experiment, meaning that the microbiome composition difference could account for changes in metabolic profiles. However, we were able to confirm some potential compounds that are significantly upregulated in both

conditions after the infection, and upon further investigation could serve as potential biomarkers for upcoming culture crashes (Fig 10)..

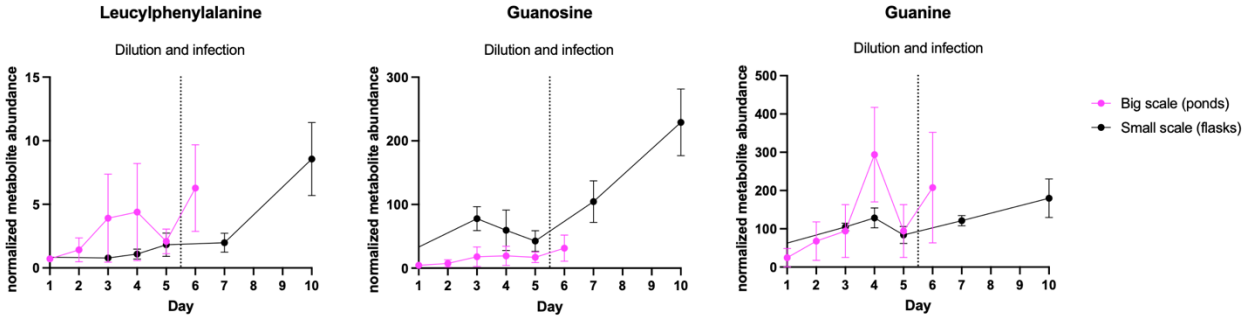

Fig. 10: Metabolites who can act as early pond crash biomarkers, verified by small-scale experiment.

3.6 Integrated multi-omic analysis revealed distinct molecular features related to scale transition and infection defense

To assess the global relationships among proteins, metabolites and transcripts across our longitudinal experiment, we performed an integrative analysis via the DIABLO framework in the mixOmics R package [38]. We performed this analysis using all omics data from days 0 and 1 to explore the molecular features of the scale-up stress, and separately used days 4 and 5 data to explore that of the infection stress. While we found that there was no overlap in the key proteins or transcripts output by the model between the scale up and infection stress, here were two metabolites, guanine and 12-oxo-Phytodienoic acid, were common across the two stressors, suggesting more convergence at the metabolite level than at the molecular pathway level.

We took the molecular features from the first latent component of both analyses and combined them into one heatmap to comprehensively visualize these results (Fig. 11). As expected, the columns clustered by day, and we observed that the two transitions had almost entirely unique patterns. We observed a cluster of transcripts (all significantly differentially expressed between days 0 and 1), proteins, and myristic acid elevated on day 0 relative to the other days. Similarly, we observed another distinct cluster of transcripts and proteins, as well as 1,5-hexadiene and 2,3-Diaminosalicylic acid, which were elevated on Day 4 compared with the other days. However, a decrease in a different cluster of proteins, as well as maltose and hypogeic acid, distinguished day 1 relative to the other days. These results suggest distinct molecular and metabolic profiles in response to different stressors, identifying potential unique biomarkers and target pathways for detection and intervention.

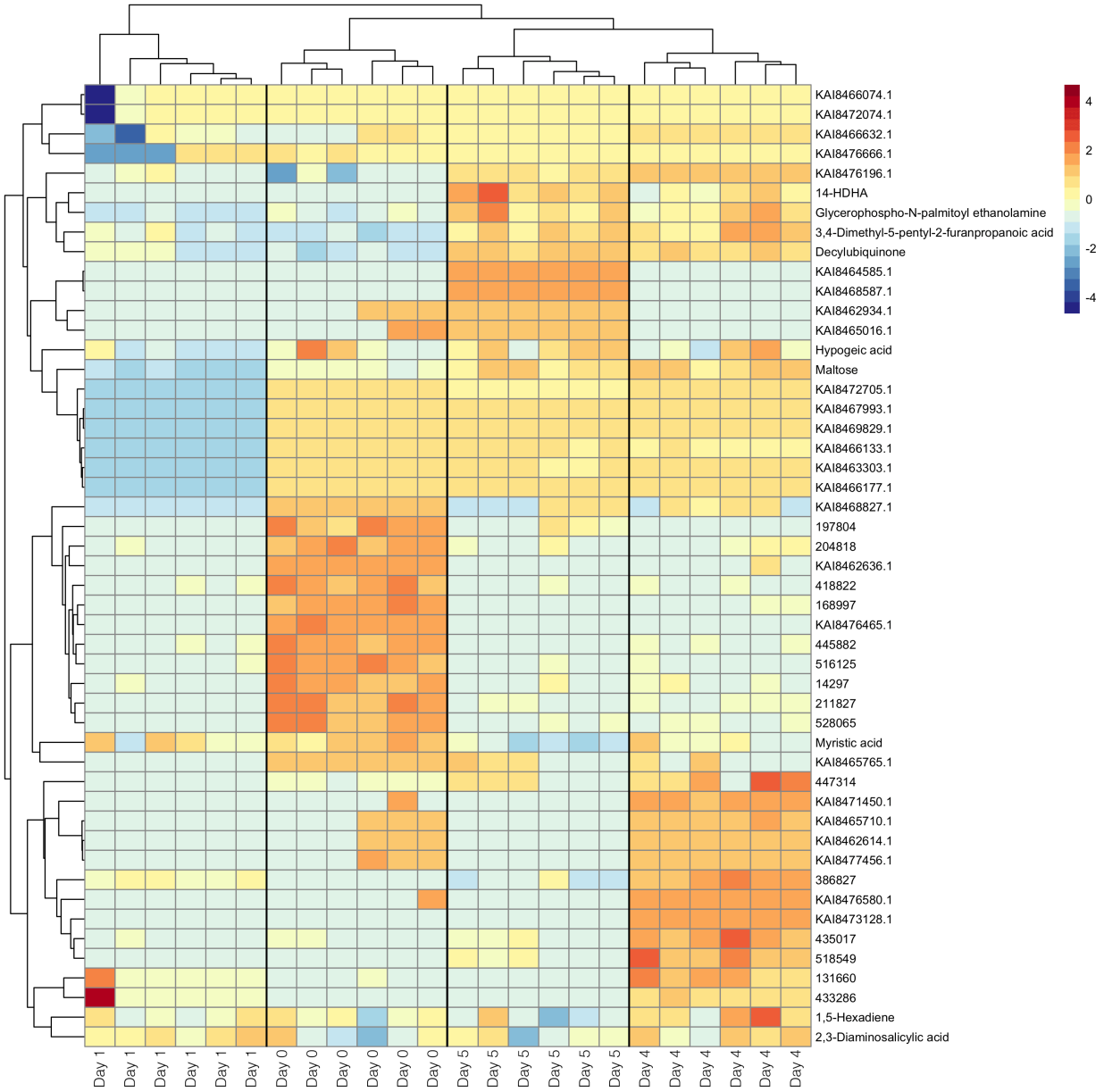

Fig. 11: Indicative signatures of scale adaptation and infection. *Heatmap containing the molecular features (genes, proteins and metabolites) which change significantly their abundance during the transition from day 0 to day 1 and/or from day 4 to day 5. Their abundance is being indicated by a scaled blue-to-red scheme. Each of the 6 biological replicates for each condition are indicated separately*

In order to determine the dynamics of the transcriptomic and proteomic observations for pathway analysis we performed a correlation analysis among the daily transcriptomic and proteomic datasets and between the two datasets (Fig.12A). The results indicate a well-expected divergence in the two datasets between the first days (corresponding to acclimation regulation) and the rest of the growth. They also showcased that the proteomics are more stable and less dynamic than the transcriptomics, and thus less sensitive as observation markers for stress events.

To integrate the various data streams and confirm the potential diverging signals and pathways across the two stress events, we wanted to demonstrate that specific genes that shared a regulatory motif partnered with proteins and metabolites to regulate distinct pathways in a stressor-specific manner. We performed a protein-protein interaction network analysis to showcase the specific networks which regulate the scale-up and the infection stresses, via STRING (Fig.12B). While common features exist in both networks, it is evident that distinct and unique interactions are significant between those two stressors, verifying our initial observations. The enlarged network figures are shown in Additional Figures 2 and 3.

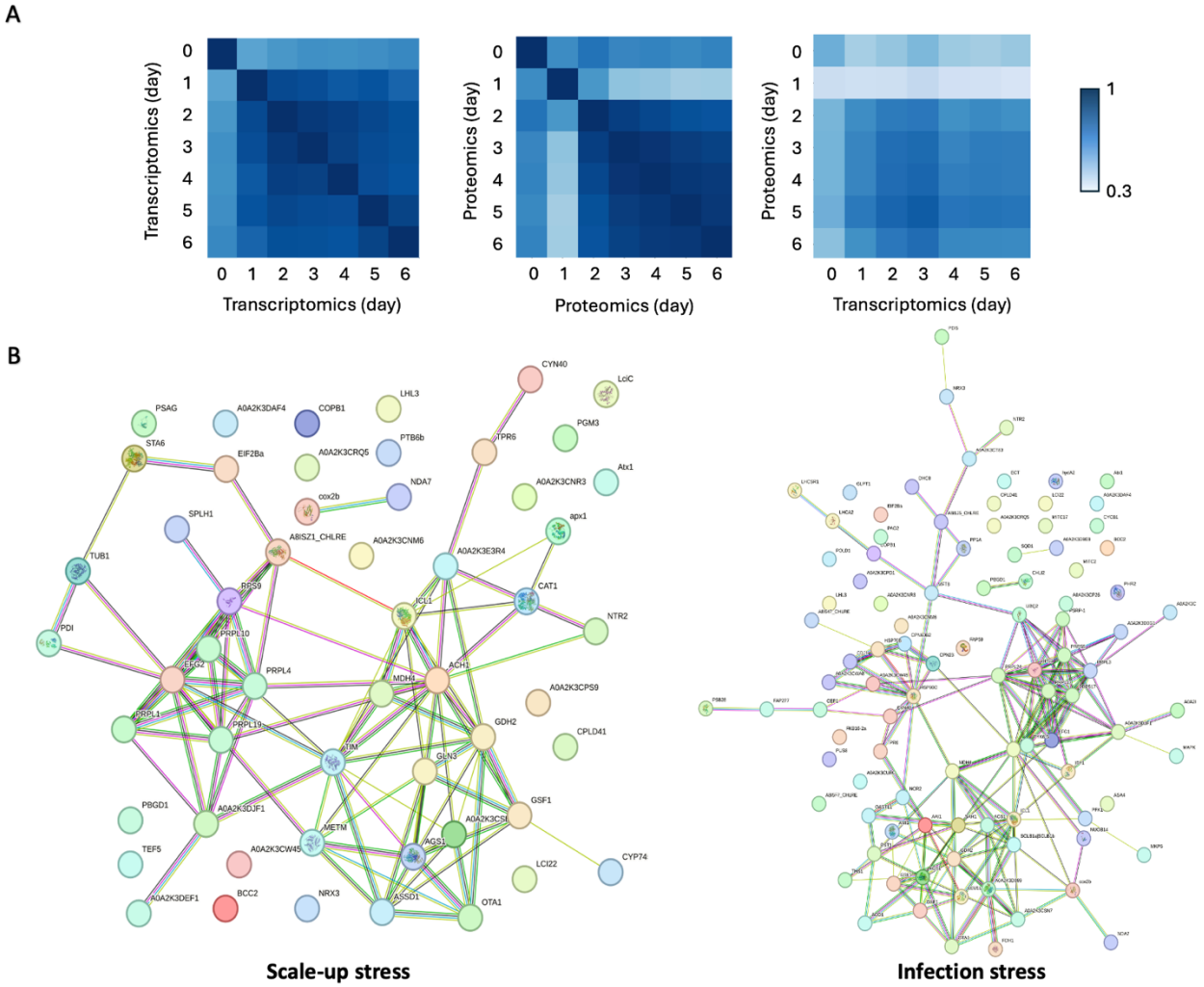

Fig.12: Understanding the dynamics between proteomic and transcriptomics observation and elucidating the individual network of features specifically related to the scale-up stress and the infection stress. *A) Heatmap with the correlation between the proteomic and transcriptomic features. B) Network of protein features, significant for the scale-up and infection stress, made through STRING.*

Specifically, we see nodes like Glutamate Dehydrogenase 2 (GDH2), Malate Dehydrogenase (MDH) and the bacterial-type polymerase AGS1 that are shared between stressors, and these genes are known to be involved in processes such as carbon and nitrogen fixation, and macromolecule biosynthesis [45]. We also see families such as Epidermal Growth Factors (EGFs) [46], the ribosomal small protein subunits (RPSs),

646 Phosphoribosylpyrophosphate Synthetases (PRPSs) [47] and the genes for prolactin (PRPLs) representing
647 the larger gene expression and translational machinery. These are common nodes between the stressors,
648 but we see different members of these families in the two stressors, suggesting that even pathways that
649 might be shared between stressors are likely controlled through different sub-pathways depending on the
650 nature of the stressor. HSPs (heat shock proteins) seem to be specific to the scale-up network, which is
651 consistent to needing to keep proteins properly folded during rapid new protein synthesis and cell cycle
652 progression during scale up [48] [49]. With amoeboaphelid infection, ICL1 (isocitrate lyase), a player in
653 the glyoxylate cycle, appears to be a unique hub, which would be consistent with re-directing metabolic
654 processes during stress as has previously been shown in other species [50] [51]. This suggests that there
655 are shared factors, shared processes with distinct factors, and distinct processes all at play for stressor-
656 specific responses, and within these pathways could lie biomarkers and countermeasure targets that are
657 either stress-specific or stress-agnostic.

658

659 **4. Discussion**

660

661 *4.1 Transcriptomics reveal the commonalities and differences between the molecular mechanisms*
662 *governing scale-up stress and infection response*

663

664 We performed a multi-omic analysis of *M. minutum* 26B-AM cultivated over 12 days in 1000 L open
665 raceway ponds to explore the molecular signatures that manifest in response to stressors often
666 encountered at a large scale. The three distinct growth phases we observed in the 1000 L ponds were in
667 line with what is typically observed at a large scale, i.e., batch cultivations of algae [52] [53]. Culture scale-
668 up is often evidenced by a lag phase, as we observed in our cultures, especially when moving from well-
669 controlled laboratory cultures into open raceway ponds [52] [54] [55]. A change in scale represents a
670 significant stressor for the cultures, introducing a combination of different environmental signals,
671 including changes in light, radiation, heat, gas distribution, as well as microbial and environmental particle
672 composition that requires an acclimation period, which is reflected in our growth curves over days 0 and
673 1.

674 Similarly, algal pests are common stressors experienced in open raceway ponds and active areas of study.
675 Changes in phenotypic measurements in response to infection or even visual indications of infection
676 stress, typically appear sometime after the initial infection. In our cultures, we introduced the
677 amoebaphelid on day 4 but did not begin to observe a decline in growth, which was emblematic of a
678 culture crash, until day 8, accompanied by a color change in the culture from light green to brown. Pond
679 crashes, which are driven by algal pathogens and often damage crops overnight, account for almost 30%
680 of algal crop losses annually [56], increasing the overall cost of algal applications. Despite the dramatic
681 effects of those infections on ponds, the cellular mechanism of the infection which includes the insertion
682 of the parasite in the host cell [19], allows a certain amount of time of incubation before a noticeable
683 crash [57]. Cellular and molecular alterations are already in place and if they can be detected in a timely
684 manner, the irreversible effects of a pond crash can potentially be avoided, or at least resource allocation
685 decisions can be made much earlier.

686 Differential expression analysis revealed that culture scale up has a substantial effect on the
687 transcriptome, as evidenced by the much larger portion of significantly differentially expressed transcripts
688 between days 0 and 1 compared with the other days, including those impacted by infection. In addition,
689 infection is not expected to trigger a wide immune response from the algal cells, reflected by
690 transcriptional adaptation. Characterizing these pathways and adjusting conditions to prevent their
691 activation could help acclimate the culture in a less stressful way and potentially make it more resilient to
692 future stressors.

693 With respect to infection, current strategies for early indication of contamination include visual detection
694 strategies such as flow cytometry [58], in situ microscopy [59], multispectral image analysis [60] and
695 photosynthetic measurements [61] [62]. Those methodologies, although relatively quick, require a certain
696 pathogen titer in the culture. Biomolecular approaches include 16S and 18S sequencing [63], and the
697 detection of Volatile Organic Compounds (VOC), as indirect early indicators of an infection [64]. Here we
698 show that the algae can also be used as early indicators of infection, as demonstrated by the changes in
699 transcripts.

700 Because many of the transcripts in *M. minutum* are poorly annotated, we used motif analysis to further
701 explore the significantly differentially expressed genes. Most identified motifs were unique to each
702 transition, potentially indicating two distinct regulatory pathways between the scale adaptation and
703 pathogen stress. However, common elements between the two datasets exist, implying that there are
704 factors that could be used to coregulate responses to different stressors (either endogenously or via
705 synthetic biology). An example of a potential point of convergence are the motifs recognized by the
706 transcription factors mitochondrial retrograde 1 (RTG1) and 3 (RTG3), both of which were originally
707 identified in yeast and are involved in mitochondrial metabolic regulation.

708 Among the promoters of genes differentially expressed during scaling up, we also identified a motif
709 labeled by HOMER as ZNF549, which is likely bound by zinc finger proteins, a family of transcription factors
710 that have been shown to regulate stress responses in other algal species [65] [66]. In addition, 31.84% of
711 the motifs correspond to a promoter motif from the diatom *Thalassiosira pseudonana* suggesting possible
712 functional importance across diverse algal species. A notably high percentage (66.66%) of the promoter
713 regions of the genes that were significantly differentially expressed after the infection contained a motif
714 that can be recognized by Auxin Response Factor 1 (ARF1), a transcription factor identified in *Arabidopsis*
715 *thaliana.* ARF1 is responsive to the phytohormone auxin, which is responsible for a wide range of
716 developmental and stress responses in plants [67] [68]. Given the evolutionary proximity between higher
717 plants and green algae, it is likely that ARF1 may have similar functions in algal responses post-infection
718 and might suggest a possible defense mechanism. The identification of these factors points to potential
719 targets for synthetic biology in *M. minutum* in the future, to either boost or tamper with specific molecular
720 responses.

721

722 *4.2 Metabolomics provide useful information about potential stress and growth biomarkers in algae*
723 *cultures*

724

725 A survey of the metabolites released by the algae upon encountering various stressors also provides
726 valuable insights into predictive markers, pond health indicators, and infection indicators, while also
727 explaining the natural mechanisms of growth and defense in algae. We used PCA and DPGP to look at
728 global trends in metabolites over time. While log phase was linked with transcriptomic stability, the
729 metabolic profile is very dynamic during the growth phase.

730 These metabolites are highly important, both as early and timely indicators of an upcoming crash and as
731 guides for the development of prophylactic strategies for algal cultures. Among those metabolites,
732 [69]there are multiple hormones and steroids (5-Dihydrotestosterone, 7-Hydroxytestosterone, Estrone,
733 Estriol and 19-Norandrostenedion). While such compounds originate in the aquatic environments from
734 sources other than algae, many algal species are known to biotransform them or completely remove them
735 from the system [70] [71] [72], with effects that can be either toxic or growth promoting for the cells [73]
736 [74].

737 As the ponds were open to environmental influence, bacterial communities present are composed of both
738 environmental bacteria and the algae-associated microbiomes living on the surface of the algal cells [75].
739 Although *M. minutum* 26B-AM has been extensively studied as a potential source of biofuels [52] [76] [77]
740 [78], there is only one other publication related to its associated microbiome during cultivation for
741 bioproducts [79]. It was described there that the bacterial community was dominated by
742 Alphaproteobacteria. No information was available from this study on eukaryotic community members
743 other than *Monoraphidium*, although since cultures were grown in outdoor raceway ponds similar to the
744 ones used in the current study, it can be assumed that there were both prokaryotic and eukaryotic
745 environmental members. Other studies of related green algae species found that bacteria might play
746 important roles in regulating nutrient dynamics and impacting cross-species interaction between
747 eukaryotic and prokaryotic community members [80] [81]. There was no statistically significant
748 relationship between any of the bacterial phyla and algal productivity, suggesting that the aphelid
749 infection was the primary driver of lowered algal productivity during the infection period. However, since
750 the aphelid was not detectable until seven days post-infection, this suggests that early pest detection
751 should rely on both molecular methods and microscopy, which may allow for earlier detection and thus a
752 longer response time for algal cultivators prior to crop loss.

753 We also identified 14-HDHA, a hydroxy docosahexaenoic acid oxylipin which is derived from
754 docosahexaenoic acid (DHA). The production of oxylipins from algae is linked with oxidative stress [54],
755 suggesting a similar regulatory pathway here for pathogen defense. When we repeated the infection
756 treatment on the flask level, we observed similar uptake on DHA post-infection. DHA is a type of omega-
757 3 fatty acid with great commercial interest of human nutrition, often produced by algal systems [82] [83]
758 [84] [85]. It has been also reported that co-cultures of algae and fungal species can improve the yield of
759 algal-produced DHA [86] [87].

760 The comparison of the metabolomics from the ponds and the flasks pre- and post- infection gave us three
761 metabolites that increase after the addition of the pathogen in both scales. Those were
762 Leucylphenylalanine, guanosine and guanine (Fig. 10). While the comparison between a big-scale open
763 system and controlled laboratory axenic environment can be confounded by environmental and
764 experimental factors, the verification of the uptake of those metabolites certifies their status as potential
765 biomarkers for upcoming culture crashes.

766

767 *4.3 Transcriptomic and phenotypical observations reflect light and gas-regulated responses in M. minutum*

768

769 Light and gas constitute the two cornerstone environmental factors for aquatic organisms, especially the
770 photosynthetic organisms such as green microalgae. Indeed, light and CO_2 availability are essential not
771 only for photosynthesis, the primary metabolic function of microalgae but also for photoprotection, lipid
772 composition, and carbon concentration [88] [89] [90] [91] [92]. The conserved and well-studied role of
773 light and CO_2 availability led us to explore which *M. minutum* genes are corelated with these conditions,
774 to test the validity of our method on identifying molecular signatures. We observed that translation-
775 related proteins were strongly correlated with high light intensity. Protein translation is an essential
776 regulatory step for phenotypic acclimation, and its control by light has been observed in other algae,
777 including the Chlorophyte *Ulva prolifera* [93], the Charophyte *Klebsormidium nitens* [94], and *Chlorella sp.*
778 [95]. In addition, we noted a gene coding for a structural component of Photosystem I among the genes
779 whose expression was downregulated in response to light. Photosystem I is a crucial component of the
780 electron transport chain and is responsible for the light-mediated transfer of electrons across the
781 thylakoid membrane. Excess light can cause oxidative stress and subsequent photoinhibition in
782 Photosystem I, and in many photosynthetic organisms, including in *Chlamydomonas reinhardtii*, light can
783 suppress the expression of structural proteins in Photosystem I to protect the machinery from this type
784 of damage [96]. Future work to test this hypothesis across algal species will be critical.

785 Motif analysis of the promoter regions of genes correlated with light highlighted two motifs related to
786 homeobox proteins in higher plants. The *Zea mays* homeobox 2a (ZmHOX2a) protein, whose expression
787 in maize is restricted to meristems, is involved in in plant development and growth [97]. In addition, this
788 motif might more broadly represent homeobox transcription factors, which are known to regulate
789 environmental responses in plants [98] [99], suggesting evolutionary conservation of light-induced gene
790 regulation through homeobox transcription factors across the plants and algae. A motif corresponding to
791 the same transcription factor is also found among the motifs from the promoters of the downregulated
792 genes by light, highlighting the involvement of these motifs in both the up- and downregulation responses
793 to light. Interestingly, 30.80% of the targets of the promoter regions from the up-regulated genes
794 contained a motif corresponding to the transcription factor RGT1 (Restores Glucose Transport) from
795 *Saccharomyces cerevisiae*. The protein regulates glucose transport though the expression of glucose
796 transporters [100], and the connection between light-induced stress and glucose transport has been
797 documented in other organisms [101] [102]. The motifs of the downregulated genes include one that is
798 recognized by the *Saccharomyces cerevisiae* stress-related multicopy suppressor of SNF1 mutation
799 protein 4 (Msn4), which controls the metabolic response under cellular stress conditions [103].

800 Among the genes correlated with DO, multiple genes are related to photosynthesis and carbon fixation.
801 A phosphoribulokinase/uridine kinase, an enzyme responsible for a key step in the Calvin-Benson cycle,
802 and a light-harvesting protein of Photosystem I are among the most upregulated genes. Genes related to
803 programmed cell death were positively correlated with DO, an observation that aligns with results from
804 other green algal species linking ROS signaling and programmed cell death [104] [105] [106] [107] [108].
805 These observations highlight specific molecular changes experienced by large-scale cultures that are likely
806 directly related to environmental fluctuations. Our results also revealed that increased DO caused more
807 gene downregulation than gene upregulation overall, especially for the genes indicated in Table 8. Most
808 of these genes are correlated with structural components of ribosomes, indicating a strong suppressive

809 relationship between O_2 levels and translational regulation, as was also observed in the case of genes
810 upregulated with light. In fact, the most downregulated gene from the DO was the most upregulated one
811 from light. Since high light is a stress factor, as is low oxygen, this reciprocal relationship between their
812 regulated genes aligns with expectations. The list of the top five downregulated genes includes a P-loop
813 containing nucleoside triphosphate hydrolase, which, in higher plants such as *Arabidopsis,* acts as a
814 signaling molecule involved in ribosome formation and attenuates ROS formation and oxidative stress
815 [109] [110].

816 Motif analysis of the promoter regions of all the genes correlated with DO revealed enrichment of the
817 binding site for the same transcription factor from the diatom *Thalassiosira pseudonana* that we observed
818 during scale acclimation. This putative transcription factor motif is found in 40.40% of the promoter
819 regions of the genes differentially expressed during scale acclimation (Table 1), which is a sign of a strong
820 contribution of the DO differences to the scale transition stress. Future efforts to identify this transcription
821 factor that is conserved across algae might be fruitful for understanding stress mechanisms and for
822 developing broad-scale synthetic biology-based interventions. The second most enriched motif among
823 the promoters of the upregulated genes corresponds to the transcription factor Arrestin 1 (ARR1), which
824 in higher plants is responsive to the phytohormones Cytokinins and plays a fundamental role in numerous
825 developmental stages of the plant [111] .The motif bound by the yeast transcription factor Regulation of
826 the Mitochondrial Retrograde 3 (RTG3) is also found at the promoters of downregulated genes. This
827 transcription factor regulates in multiple metabolic pathways, including amino acid and nucleotide
828 synthesis [112] indicating a possible role of oxygen-regulated metabolic responses in *Monoraphidium*.
829 Interestingly, motifs corresponding to the same transcription factor were found among the photometers
830 of the differentially expressed genes during the acclimation period and after the infection with the
831 amoeboapheids (Tables 1 and 2), which implies a role for transcription factors that bind this motif across
832 stressors and environmental changes.

833 We also noted that we identified overlap in the genes correlated with light and DO and those related to
834 stress responses (specifically responses to cold and salt), as determined by [17]. Specifically, of the 24
835 genes they outline as being annotated with a fasciclin-like domain, a domain with known roles in algal and
836 plant stress responses, we note 2 with expression coordinated with dissolved oxygen (annotation #
837 450375, 525465), 1 with expression coordinated with light (annotation # 480939) and 2 with expression
838 levels coordinated with both (annotation # 421681, 446308). These results support the validity of our
839 signature identification through multi-omic data integration in algae, and point towards the need for
840 follow-up on our stress signatures for identification of predictive markers for tracking large-scale pond
841 culture resiliency, and molecules for therapeutic intervention.

842

843 **5. Conclusions**

844

845 In this study, we used multi-omics to investigate the dynamic responses of the green alga *M. minutum* to
846 various environmental changes and stressors. A study of multi-omic analyses of *M. minutum* was recently
847 published, providing a molecular profile of this industrially significant species under high salt and cold
848 temperature stress [17]. We utilized a multi-omic approach in larger open and, thus, more heterogeneous
849 culture systems in order to provide a roadmap for the application of molecular observations at the cellular

level and data processing to address the significant challenges faced by the large-scale bioprocessing industry. [57, 113]Our approach aims to address these issues while gaining information about the cellular responses of the species. We demonstrated the ability to integrate datasets of genes, proteins and metabolites that respond to specific stressors or correspond to certain culture stages and transitions, opening up possibilities for follow-up studies in the fields of strain engineering, biomarker development, bioprocessing, and basic cellular studies.

We can begin to build an integrated model to understand how *M. minutum* responds to two key stressors by integrating all the multi-omic information obtained, as outlined in Fig. 13. While we found that a number of genes contained common motifs (such as RTG, a stress factor that has been extensively studied in yeast [114] [115] [116]), we focused on the genes with the two most prominent motifs from our motif analysis ARF1 (highly enriched in scale-up stress) and an unannotated *Thalassiosira pseudonana* factor (T.p). We performed pathway analysis with the use of GPT-4, as suggested on [39], and see pathways consistent with the hubs of protein-protein interaction identified in Fig. 12. Taken together we have candidate genes, proteins and metabolites to target both for biomarker-based detection and for countermeasure and mitigation development.

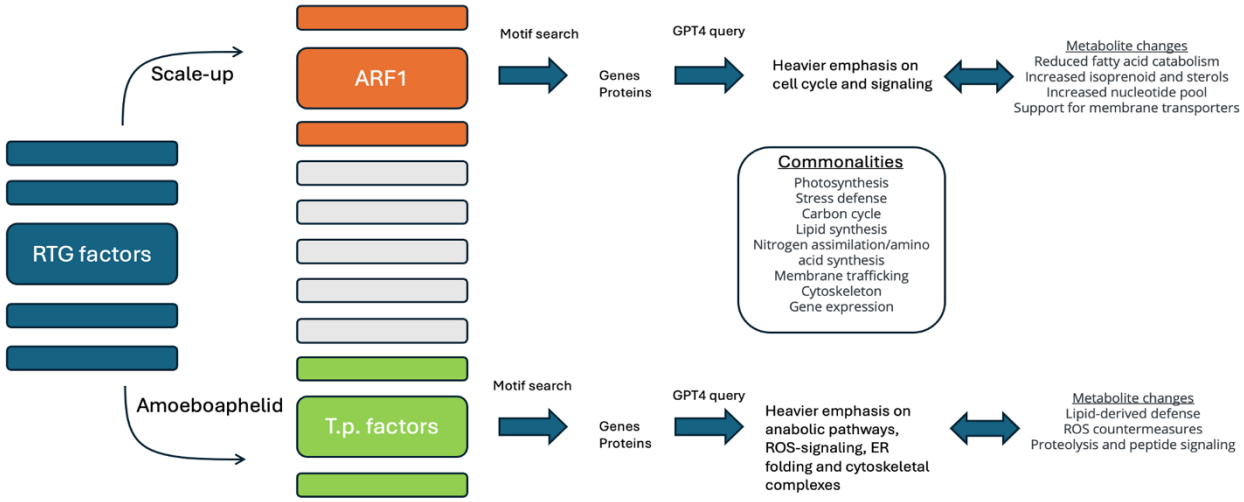

Fig.13: Procedural explanation of the use of GPT4 for stress-related regulation and metabolic changes.

With respect to metabolites in particular, for example, which are the most likely candidates for biomarker detection and immediate therapeutic intervention, specific hormones and steroids, such as 5-Dihydrotestosterone, 7-Hydroxytestosterone, Estrone, Estriol and 19-Norandrostenedion, are highly expressed during early infection. [73, 117, 118]Given that their abundance increased after the introduction of the pathogen, showcases that those compounds can be utilized as timely biomarkers for upcoming pond crashes. In the long term, if some of these molecules act in defense against algae, microbiomes can be engineered to produce these molecules as a prophylactic strategy during large-scale culture.

On a broader scale, the collection of molecular data from such expansive cultivation systems can pave the way for analyses aimed at developing predictive power with respect to culture resiliency, as well as potential targets for engineering this resiliency in the future. Indeed, we observed transcripts shared in both this study and the study conducted by Calhoun et al (2022), which indicates that more data generation in small- and large-scale systems, coupled with integrated analysis, could reveal novel health monitoring molecules in algal culture. The ultimate goal is for these models to be adaptable to multiple types of bioprocessing, beyond algae cultures, and this study provides a roadmap in that direction, using omic data to optimize large-scale applications.

Abbreviations

14-HDHA: 14-hydroxy-docosahexaenoic acid

AFDW: Ash-free dry weight

ARF1: ADP-ribosylation factor 1

ARR1: Arabidopsis response regulator 1

CCM: Carbon concentration mechanism

DIABLO: Data Integration Analysis for Biomarker discovery using Latent Components

DISCOVR: Development of integrated screening, cultivar optimization, and verification research

DPGP: Dirichlet Process Gaussian Process mixture model

Msn4: multicopy suppressor of SNF1 mutation protein 4

PCA: principal component analysis

ROS: reactive oxygen species

RuBisCO: Ribulose-1,5-bisphosphate carboxylase/oxygenase

RTG1: mitochondrial retrograde 1

RTG3: mitochondrial retrograde 3

SNF1: sucrose non-fermenting 1

Declarations

Ethics approval and consent to participate

N/A

Consent for publication

N/A

Availability of data and materials

The datasets supporting the conclusions of this article are available in the NCBI SRA repository, under BioProject PRJNA1307767 and are included within the article and its additional files.

Competing interests

The authors declare that they have no competing interests.

Funding

This work was supported by the DOE Bioenergy Technology Office (BETO) and the Laboratory Directed Research and Development program at Sandia National Laboratories, a multimission laboratory managed and operated by National Technology and Engineering Solutions of Sandia LLC, a wholly owned subsidiary of Honeywell International Inc. for the U.S. Department of Energy's National Nuclear Security Administration under contract DE-NA0003525.

Authors' contributions

R.K. led the funding acquisition efforts and had the logistic and programmatic lead of the project. G.K and R.K. conceptualized the project and designed the methodology and the experimental procedure. G.K., D.Y., E.W., T.E., O.W. and M.P.H. worked on the different aspects of the experimental procedure (scale-up, pond running and maintenance, sampling and phenotyping, omics preparation and sequencing). G.K., J.S., D.Y., T.S. and R.K. worked on the computational and bioinformatic analysis. T.W.L. advised on the experimental design and algal physiology. G.K, J.S. and R.K. wrote the original manuscript. All the authors reviewed and edited the manuscript.

Acknowledgements

This paper describes objective technical results and analysis. Any subjective views or opinions that might be expressed in the paper do not necessarily represent the views of the U.S. Department of Energy or the United States Government. We thank Ryan W. Davis, Catherine Mageeney, Pamela Lane, and Carolyn Fisher, Sharon Nademanee, and Damian Carrieri for their insightful comments on an earlier draft of this manuscript.

942 **Additional data**

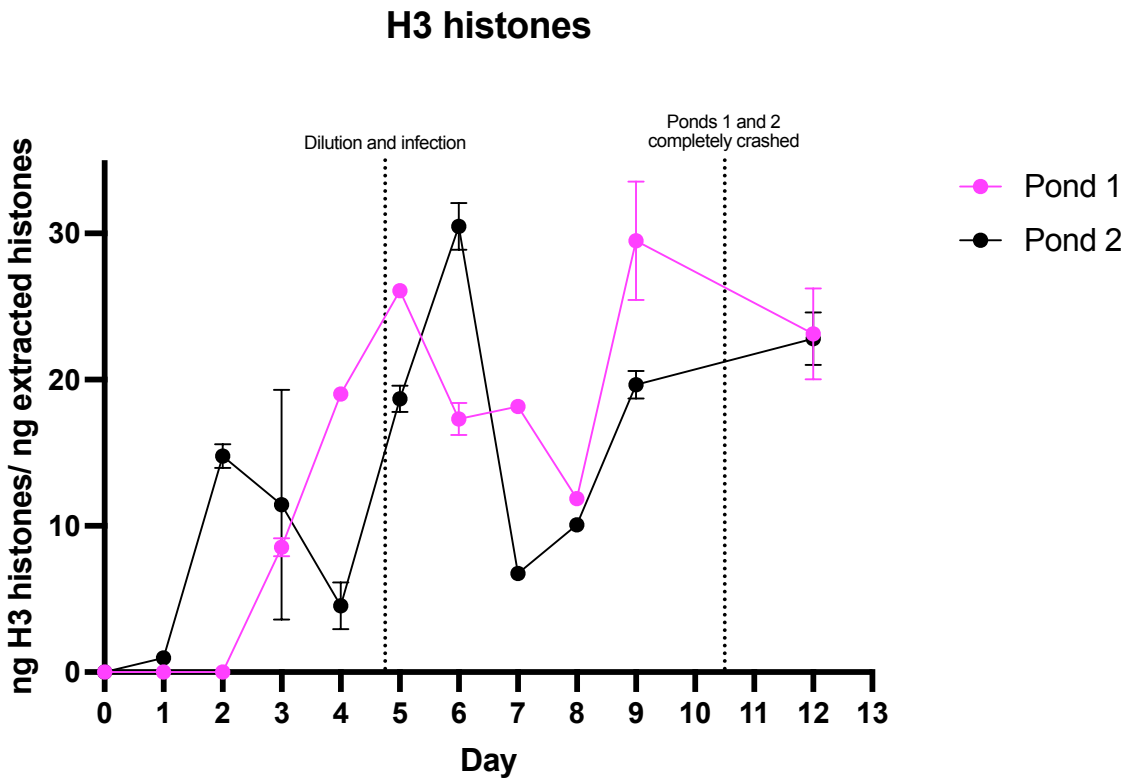

943

944 ***Additional Figure. 1: The caspase activity during the pond run.*** *The caspase activity for every day of the culture run in pond 1*
945 *(pink) and pond 2 (black).*

946

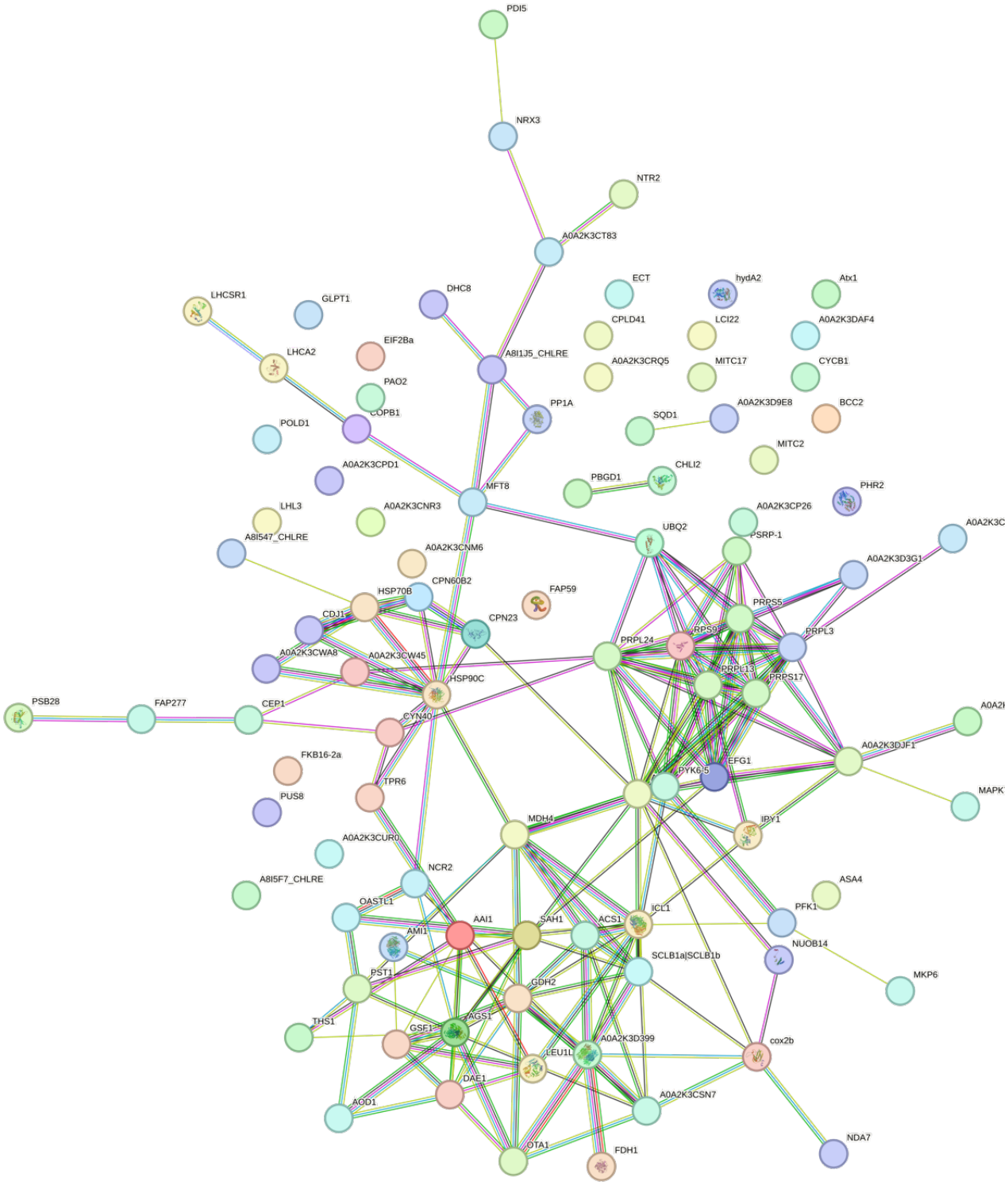

947

948 ***Additional Figure 2: The complete STRING protein-protein network for the significant features during the scale-up stress***

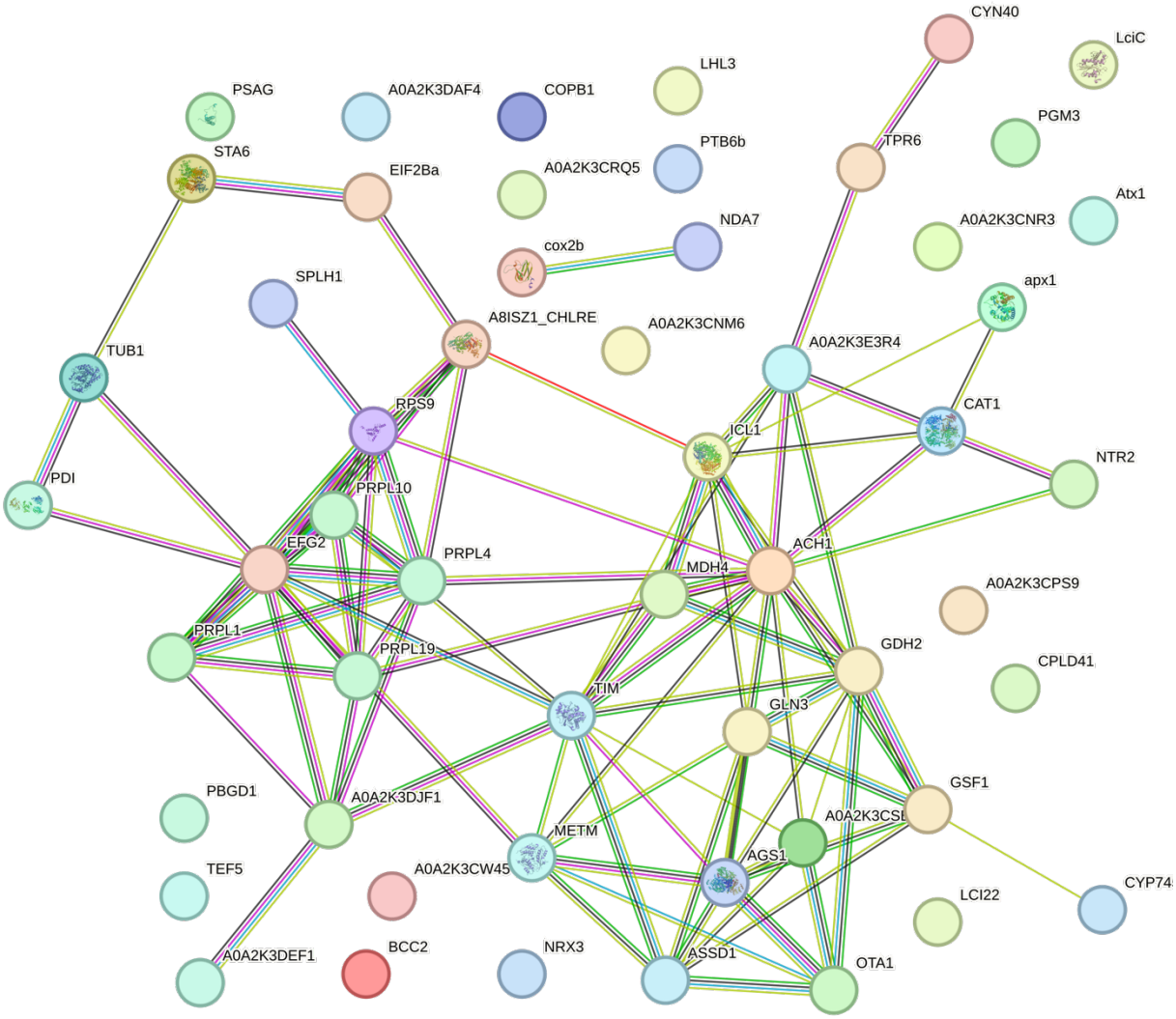

Additional Figure 3: The complete STRING protein-protein network for the significant features during the infection stress.

Additional Dataset 1: Phenomics

Additional Dataset 2: Metagenomics

Additional Dataset 3: Transcriptomics

Additional Dataset 4: Proteomics

Additional Dataset 5: Metabolomics

Additional Dataset 6: Metabolomics small scale

References

1. Dismukes, G.C., et al., *Aquatic phototrophs: efficient alternatives to land-based crops for biofuels.* Current Opinion in Biotechnology, 2008. **19**(3): p. 235-240.
2. Cruce, J.R. and J.C. Quinn, *Economic viability of multiple algal biorefining pathways and the impact of public policies.* Applied Energy, 2019. **233-234**: p. 735-746.
3. Thanigaivel, S., et al., *The urge of algal biomass-based fuels for environmental sustainability against a steady tide of biofuel conflict analysis: Is third-generation algal biorefinery a boon?* Fuel, 2022. **317**: p. 123494.
4. Wiatrowski, M., et al., *Techno-economic assessment for the production of algal fuels and value-added products: opportunities for high-protein microalgae conversion.* Biotechnology for Biofuels and Bioproducts, 2022. **15**(1): p. 8.
5. Costa, J.A.V., et al., *Chapter 9 - Open pond systems for microalgal culture*, in *Biofuels from Algae (Second Edition)*, A. Pandey, et al., Editors. 2019, Elsevier. p. 199-223.
6. Jerney, J. and K. Spilling, *Large Scale Cultivation of Microalgae: Open and Closed Systems*, in *Biofuels from Algae: Methods and Protocols*, K. Spilling, Editor. 2020, Springer New York: New York, NY. p. 1-8.
7. Lane, T.W., *Barriers to microalgal mass cultivation.* Current Opinion in Biotechnology, 2022. **73**: p. 323-328.
8. Quiroz, D., et al., *Geographical assessment of open pond algal productivity and evaporation losses across the United States.* Algal Research, 2021. **60**: p. 102483.
9. Echenique-Subiabre, I., et al., *Site-specific factors override local climatic conditions in determining microalgae productivity in open raceway ponds.* Algal Research, 2023. **74**: p. 103235.
10. Kleiman, R.M., et al., *Characterizing weather-related biophysical and financial risks in algal biofuel production.* Applied Energy, 2021. **294**: p. 116960.
11. Borowitzka, M. and A. Vonshak, *Scaling up microalgal cultures to commercial scale.* European Journal of Phycology, 2017. **52**: p. 407-418.
12. Patidar, S.K., et al., *Potential of Monoraphidium minutum for carbon sequestration and lipid production in response to varying growth mode.* Bioresource Technology, 2014. **172**: p. 32-40.
13. Dommange, X., P.A. Tanguy, and M. Jolicoeur, *Feasibility of lipid mechanical extraction from viable Monoraphidium minutum.* Microalgae Biotechnol, 2015. **1**(1): p. 12-19.
14. Bogen, C., et al., *Reconstruction of the lipid metabolism for the microalga Monoraphidium neglectum from its genome sequence reveals characteristics suitable for biofuel production.* BMC genomics, 2013. **14**: p. 1-18.
15. Yu, X., et al., *Isolation of a novel strain of Monoraphidium sp. and characterization of its potential application as biodiesel feedstock.* Bioresource Technology, 2012. **121**: p. 256-262.
16. Pikoli, M.R., et al., *Characteristics of tropical freshwater microalgae Micractinium conductrix, Monoraphidium sp. and Choricystis parasitica, and their potency as biodiesel feedstock.* Heliyon, 2019. **5**(12).
17. Calhoun, S., et al., *Multi-omics profiling of the cold tolerant Monoraphidium minutum 26B-AM in response to abiotic stress.* Algal Research, 2022. **66**: p. 102794.
18. Mikhailov, K.V., et al., *Genomic analysis reveals cryptic diversity in aphelids and sheds light on the emergence of Fungi.* Current Biology, 2022. **32**(21): p. 4607-4619.e7.
19. Letcher, P.M., et al., *Characterization of Amoeboaphelidium protococcarum, an Algal Parasite New to the Cryptomycota Isolated from an Outdoor Algal Pond Used for the Production of Biofuel.* PLOS ONE, 2013. **8**(2): p. e56232.

1007 20. Huesemann, M., et al., *DISCOVR strain pipeline screening – Part I: Maximum specific growth rate*
1008 *as a function of temperature and salinity for 38 candidate microalgae for biofuels production.* Algal
1009 Research, 2023. **71**: p. 102996.
1010 21. Van Wychen, S. and L.M.L. Laurens, *Determination of Total Solids and Ash in Algal Biomass:*
1011 *Laboratory Analytical Procedure (LAP)*. 2016, National Renewable Energy Lab. (NREL), Golden, CO
1012 (United States): United States. p. Medium: ED; Size: 415 KB.
1013 22. Sakai, M., et al., *Application of a new PCR primer for terminal restriction fragment length*
1014 *polymorphism analysis of the bacterial communities in plant roots.* J Microbiol Methods, 2004.
1015 **59**(1): p. 81-9.
1016 23. Turner, S., et al., *Investigating deep phylogenetic relationships among cyanobacteria and plastids*
1017 *by small subunit rRNA sequence analysis.* J Eukaryot Microbiol, 1999. **46**(4): p. 327-38.
1018 24. Stoeck, T., et al., *Multiple marker parallel tag environmental DNA sequencing reveals a highly*
1019 *complex eukaryotic community in marine anoxic water.* Mol Ecol, 2010. **19 Suppl 1**: p. 21-31.
1020 25. Lu, J., et al., *Metagenome analysis using the Kraken software suite.* Nat Protoc, 2022. **17**(12): p.
1021 2815-2839.
1022 26. Lu, J., et al., *Bracken: estimating species abundance in metagenomics data.* PeerJ Comput Sci,
1023 2017. **3**.
1024 27. Wood, D.E., J. Lu, and B. Langmead, *Improved metagenomic analysis with Kraken 2.* Genome Biol,
1025 2019. **20**(1): p. 257.
1026 28. Quast, C., et al., *The SILVA ribosomal RNA gene database project: improved data processing and*
1027 *web-based tools.* Nucleic Acids Res, 2013. **41**(Database issue): p. D590-6.
1028 29. Demichev, V., et al., *DIA-NN: neural networks and interference correction enable deep proteome*
1029 *coverage in high throughput.* Nature Methods, 2020. **17**(1): p. 41-44.
1030 30. Kassambara, A. and F. Mundt. *Extract and Visualize the Results of Multivariate Data Analyses [R*
1031 *package factoextra version 1.0.7]*. 2020.
1032 31. Bolger, A.M., M. Lohse, and B. Usadel, *Trimmomatic: a flexible trimmer for Illumina sequence data.*
1033 Bioinformatics, 2014. **30**(15): p. 2114-20.
1034 32. Bray, N.L., et al., *Near-optimal probabilistic RNA-seq quantification.* Nature Biotechnology, 2016.
1035 **34**(5): p. 525-527.
1036 33. Pimentel, H., et al., *Differential analysis of RNA-seq incorporating quantification uncertainty.*
1037 Nature Methods, 2017. **14**(7): p. 687-690.
1038 34. Zhou, X. and M. Stephens, *Genome-wide efficient mixed-model analysis for association studies.*
1039 Nat Genet, 2012. **44**(7): p. 821-4.
1040 35. Wickham, H., *ggplot2: Elegant Graphics for Data Analysis.* Springer-Verlag New York, 2016.
1041 36. Kolde, R., *pheatmap: Pretty Heatmaps.* 2025.
1042 37. Heinz, S., et al., *Simple combinations of lineage-determining transcription factors prime cis-*
1043 *regulatory elements required for macrophage and B cell identities.* Mol Cell, 2010. **38**(4): p. 576-
1044 89.
1045 38. Rohart, F., et al., *mixOmics: An R package for 'omics feature selection and multiple data*
1046 *integration.* PLOS Computational Biology, 2017. **13**(11): p. e1005752.
1047 39. Azam, M., et al., *A Comprehensive Evaluation of Large Language Models in Mining Gene*
1048 *Interactions and Pathway Knowledge.* bioRxiv, 2024.
1049 40. Dho, S.H., et al., *Caspases as master regulators of programmed cell death: apoptosis, pyroptosis*
1050 *and beyond.* Experimental & Molecular Medicine, 2025. **57**(6): p. 1121-1132.
1051 41. Vavilala, S.L., et al., *KCl induces a caspase-independent programmed cell death in the unicellular*
1052 *green chlorophyte Chlamydomonas reinhardtii (Chlorophyceae).* Phycologia, 2016. **55**(4): p. 378-
1053 392.

42. Zuppini, A., et al., *Chlorella saccharophila cytochrome f and its involvement in the heat shock response.* Journal of Experimental Botany, 2009. **60**(14): p. 4189-4200.
43. Teramoto, H., et al., *Light-intensity-dependent expression of Lhc gene family encoding light-harvesting chlorophyll-a/b proteins of photosystem II in Chlamydomonas reinhardtii.* Plant Physiol, 2002. **130**(1): p. 325-33.
44. McDowell, I.C., et al., *Clustering gene expression time series data using an infinite Gaussian process mixture model.* PLOS Computational Biology, 2018. **14**(1): p. e1005896.
45. Chen, Y., et al., *Cytosolic malate dehydrogenase 4 modulates cellular energetics and storage reserve accumulation in maize endosperm.* Plant Biotechnology Journal, 2020. **18**(12): p. 2420-2435.
46. Higginbotham, J.N., et al., *Identification and characterization of EGF receptor in individual exosomes by fluorescence-activated vesicle sorting.* Journal of Extracellular Vesicles, 2016. **5**(1): p. 29254.
47. Jung, S., et al., *Overexpression of Phosphoribosyl Pyrophosphate Synthase Enhances Resistance of Chlamydomonas to Ionizing Radiation.* Front Plant Sci, 2021. **12**: p. 719846.
48. Schulz-Raffelt, M., M. Lodha, and M. Schroda, *Heat shock factor 1 is a key regulator of the stress response in Chlamydomonas.* Plant J, 2007. **52**(2): p. 286-95.
49. Kobayashi, Y., et al., *Algae sense exact temperatures: small heat shock proteins are expressed at the survival threshold temperature in Cyanidioschyzon merolae and Chlamydomonas reinhardtii.* Genome Biol Evol, 2014. **6**(10): p. 2731-40.
50. Zhang, N., et al., *Systems-wide analysis revealed shared and unique responses to moderate and acute high temperatures in the green alga Chlamydomonas reinhardtii.* Communications Biology, 2022. **5**(1): p. 460.
51. Valledor, L., et al., *Systemic cold stress adaptation of Chlamydomonas reinhardtii.* Mol Cell Proteomics, 2013. **12**(8): p. 2032-47.
52. Gao, S., et al., *DISCOVR strain screening pipeline – Part III: Strain evaluation in outdoor raceway ponds.* Algal Research, 2023. **70**: p. 102990.
53. Yang, H., Q. He, and C. Hu, *Feasibility of biodiesel production and CO2 emission reduction by Monoraphidium dybowskii LB50 under semi-continuous culture with open raceway ponds in the desert area.* Biotechnology for Biofuels, 2018. **11**(1): p. 82.
54. Huesemann, M., et al., *A validated model to predict microalgae growth in outdoor pond cultures subjected to fluctuating light intensities and water temperatures.* Algal Research, 2016. **13**: p. 195-206.
55. Matula, E.E. and D.J.A. Nability, *Metabolic response of Chlorella vulgaris to a transient thermal environment for supporting simultaneous air revitalization and thermal control in a crewed habitat.* Acta Astronautica, 2021. **187**: p. 406-415.
56. McBride, R.C., et al., *Contamination Management in Low Cost Open Algae Ponds for Biofuels Production.* Industrial Biotechnology, 2014. **10**(3): p. 221-227.
57. Harmon, V.L., et al., *Reliability metrics and their management implications for open pond algae cultivation.* Algal Research, 2021. **55**: p. 102249.
58. Ioc Coi Coi, M., et al., *Microscopic and molecular methods for quantitative phytoplankton analysis IOC. Manuals and guides*.
59. Havlik, I., et al., *Monitoring of microalgal cultivations with on-line, flow-through microscopy.* Algal Research, 2013. **2**(3): p. 253-257.
60. Murphy, T.E., K. Macon, and H. Berberoglu, *Rapid algal culture diagnostics for open ponds using multispectral image analysis.* Biotechnology Progress, 2014. **30**(1): p. 233-240.

61. Deore, P., et al., *Non-photochemical quenching, a non-invasive probe for monitoring microalgal grazing: an early indicator of predation by Oxyrrhis marina and Euplotes sp.* Applied Phycology, 2020. **1**(1): p. 20-31.
62. Fundel, B., et al., *Can phaeopigments be used as markers for Daphnia grazing in Lake Constance?* Journal of Plankton Research, 1998. **20**(8): p. 1449-1462.
63. Bartley, M.L., et al., *Effects of salinity on growth and lipid accumulation of biofuel microalga Nannochloropsis salina and invading organisms.* Biomass and Bioenergy, 2013. **54**: p. 83-88.
64. Reese, K.L., et al., *Chemical Profiling of Volatile Organic Compounds in the Headspace of Algal Cultures as Early Biomarkers of Algal Pond Crashes.* Scientific Reports, 2019. **9**(1): p. 13866.
65. Xie, J., et al., *Genome-Wide Identification and Functional Analysis of C2H2 Zinc Finger Transcription Factor Genes in the Intertidal Macroalga Pyropia haitanensis.* Int J Mol Sci, 2025. **26**(9).
66. Thiriet-Rupert, S., et al., *Transcription factors in microalgae: genome-wide prediction and comparative analysis.* BMC Genomics, 2016. **17**(1): p. 282.
67. Liu, L., et al., *Enigmatic role of auxin response factors in plant growth and stress tolerance.* Front Plant Sci, 2024. **15**: p. 1398818.
68. Ulmasov, T., G. Hagen, and T.J. Guilfoyle, *ARF1, a Transcription Factor That Binds to Auxin Response Elements.* Science, 1997. **276**(5320): p. 1865-1868.
69. Linares-Maurizi, A., et al., *Stress-Induced Production of Bioactive Oxylipins in Marine Microalgae.* Mar Drugs, 2024. **22**(9).
70. Lai, K.M., M.D. Scrimshaw, and J.N. Lester, *Biotransformation and bioconcentration of steroid estrogens by Chlorella vulgaris.* Appl Environ Microbiol, 2002. **68**(2): p. 859-64.
71. Shi, W., et al., *Removal of estrone, 17alpha-ethinylestradiol, and 17beta-estradiol in algae and duckweed-based wastewater treatment systems.* Environ Sci Pollut Res Int, 2010. **17**(4): p. 824-33.
72. Liu, D., et al., *Biochemical responses of freshwater microalgae Chlorella sorokiniana to combined exposure of Zn(Ⅱ) and estrone with simultaneous pollutants removal.* J Environ Manage, 2023. **348**: p. 119392.
73. Yu, H., et al., *Exploring the molecular mechanism of Chlorella vulgaris in response to androstenedione exposure based on genes continuously up-regulated in transcription analysis.* Ecotoxicology and Environmental Safety, 2024. **271**: p. 115996.
74. Czarny, K., et al., *Toxicity of single steroid hormones and their mixtures toward the cyanobacterium Microcystis aeruginosa.* Journal of Applied Phycology, 2019. **31**(6): p. 3537-3544.
75. Abdul Malik, S., et al., *Screening of Surface-Associated Bacteria from the Mexican Red Alga Halymenia floresii for Quorum Sensing Activity.* Microbiology, 2020. **89**: p. 778-788.
76. Huesemann, M., et al., *DISCOVR strain pipeline screening – Part I: Maximum specific growth rate as a function of temperature and salinity for 38 candidate microalgae for biofuels production.* Algal Research, 2023. **71**: p. 102996.
77. Huesemann, M., et al., *DISCOVR strain pipeline screening – Part II: Winter and summer season areal productivities and biomass compositional shifts in climate-simulation photobioreactor cultures.* Algal Research, 2023. **70**: p. 102948.
78. McGowen, J., et al., *Outdoor annual algae productivity improvements at the pre-pilot scale through crop rotation and pond operational management strategies.* Algal Research, 2023. **70**: p. 102995.
79. Wahlen, B.D., et al., *Effect of nitrogen management in cultivation on the stability and microbial community of post-harvest Monoraphidium sp. algae biomass.* J Ind Microbiol Biotechnol, 2023. **50**(1).

80. Jackrel, S.L., et al., *Microbiomes Reduce Their Host's Sensitivity to Interspecific Interactions.* mBio, 2020. **11**(1).
81. Mattsson, L., et al., *Functional Diversity Facilitates Stability Under Environmental Changes in an Outdoor Microalgal Cultivation System.* Frontiers in Bioengineering and Biotechnology, 2021. **Volume 9 - 2021**.
82. Pyle, D.J., R.A. Garcia, and Z. Wen, *Producing Docosahexaenoic Acid (DHA)-Rich Algae from Biodiesel-Derived Crude Glycerol: Effects of Impurities on DHA Production and Algal Biomass Composition.* Journal of Agricultural and Food Chemistry, 2008. **56**(11): p. 3933-3939.
83. Park, W.-K., et al., *Economical DHA (Docosahexaenoic acid) production from Aurantiochytrium sp. KRS101 using orange peel extract and low cost nitrogen sources.* Algal Research, 2018. **29**: p. 71-79.
84. Manikan, V., et al., *A new strain of docosahexaenoic acid producing microalga from Malaysian coastal waters.* Algal Research, 2015. **9**: p. 40-47.
85. Rumiani, L.A., H. Jalili, and A. Amrane, *Enhanced docosahexaenoic acid production by Crypthecodinium cohnii under combined stress in two-stage cultivation with date syrup based medium.* Algal Research, 2018. **34**: p. 75-81.
86. Du, Z.Y., et al., *Enhancing oil production and harvest by combining the marine alga Nannochloropsis oceanica and the oleaginous fungus Mortierella elongata.* Biotechnol Biofuels, 2018. **11**: p. 174.
87. Sahin, D., U.H. Altindag, and E. Tas, *Enhancement of docosahexaenoic acid (DHA) and beta-carotene production in Schizochytrium sp. using symbiotic relationship with Rhodotorula glutinis.* Process Biochemistry, 2018. **75**: p. 10-15.
88. Yamaoka, Y., et al., *Light, CO2, and carbon storage in microalgae.* Current Opinion in Plant Biology, 2025. **84**: p. 102696.
89. Tokutsu, R., et al., *Isolation of photoprotective signal transduction mutants by systematic bioluminescence screening in Chlamydomonas reinhardtii.* Sci Rep, 2019. **9**(1): p. 2820.
90. Ruiz-Sola, M.Á., et al., *Light-independent regulation of algal photoprotection by CO2 availability.* Nature Communications, 2023. **14**(1): p. 1977.
91. Maltsev, Y., et al., *Influence of Light Conditions on Microalgae Growth and Content of Lipids, Carotenoids, and Fatty Acid Composition.* Biology (Basel), 2021. **10**(10).
92. Dao, O., et al., *The green algae CO2 concentrating mechanism and photorespiration jointly operate during acclimation to low CO2.* Nature Communications, 2025. **16**(1): p. 5296.
93. Jahan, K., et al., *Transcriptomic Analysis Provides New Insights into the Tolerance Mechanisms of Green Macroalgae Ulva prolifera to High Temperature and Light Stress.* Biology, 2024. **13**(9): p. 725.
94. Serrano-Pérez, E., et al., *Transcriptomic and Metabolomic Response to High Light in the Charophyte Alga Klebsormidium nitens.* Frontiers in Plant Science, 2022. **13**.
95. Wang, B., et al., *Cell damage repair mechanism in a desert green algae Chlorella sp. against UV-B radiation.* Ecotoxicology and Environmental Safety, 2022. **242**: p. 113916.
96. Nama, S., et al., *High light induced changes in organization, protein profile and function of photosynthetic machinery in Chlamydomonas reinhardtii.* Journal of Photochemistry and Photobiology B: Biology, 2015. **152**: p. 367-376.
97. Kirch, T., et al., *The two homeodomains of the ZmHox2a gene from maize originated as an internal gene duplication and have evolved different target site specificities.* Nucleic Acids Res, 1998. **26**(20): p. 4714-20.
98. Bondino, H.G. and E.M. Valle, *A small intergenic region drives exclusive tissue-specific expression of the adjacent genes in Arabidopsis thaliana.* BMC Mol Biol, 2009. **10**: p. 95.

99. Ejaz, M., et al., *ARABIDOPSIS THALIANA HOMEOBOX GENE 1 controls plant architecture by locally restricting environmental responses.* Proc Natl Acad Sci U S A, 2021. **118**(17).
100. Polish, J.A., J.-H. Kim, and M. Johnston, *How the Rgt1 Transcription Factor of Saccharomyces cerevisiae Is Regulated by Glucose.* Genetics, 2005. **169**(2): p. 583-594.
101. Valifard, M., et al., *The novel chloroplast glucose transporter pGlcT2 affects adaptation to extended light periods.* Journal of Biological Chemistry, 2023. **299**(6): p. 104741.
102. Powner, M.B. and G. Jeffery, *Light stimulation of mitochondria reduces blood glucose levels.* Journal of Biophotonics, 2024. **17**(5): p. e202300521.
103. Rajvanshi, P.K., M. Arya, and R. Rajasekharan, *The stress-regulatory transcription factors Msn2 and Msn4 regulate fatty acid oxidation in budding yeast.* J Biol Chem, 2017. **292**(45): p. 18628-18643.
104. Al-Azab, A.J.S., et al., *Chronological transcriptome changes induced by exposure to cyanoacrylate resin nanoparticles in Chlamydomonas reinhardtii with a focus on ROS development and cell wall lysis-related genes.* Algal Research, 2022. **68**: p. 102884.
105. Gao, Y. and D.L. Erdner, *Cell death responses to acute high light mediated by non-photochemical quenching in the dinoflagellate Karenia brevis.* Scientific Reports, 2022. **12**(1): p. 14081.
106. Xu, C., et al., *Programmed cell death process in freshwater Microcystis aeruginosa and marine Phaeocystis globosa induced by a plant derived allelochemical.* Science of The Total Environment, 2022. **838**: p. 156055.
107. Bai, F., et al., *Paraquat induces different programmed cell death patterns in Microcystis aeruginosa and Chlorella luteoviridis.* Ecotoxicology and Environmental Safety, 2023. **249**: p. 114429.
108. Zhao, Y., et al., *ROS-mediated programmed cell death (PCD) of Thalassiosira pseudonana under the stress of BDE-47.* Environmental Pollution, 2020. **262**: p. 114342.
109. Zhao, M.G., Q.Y. Tian, and W.H. Zhang, *Nitric oxide synthase-dependent nitric oxide production is associated with salt tolerance in Arabidopsis.* Plant Physiol, 2007. **144**(1): p. 206-17.
110. Moreau, M., et al., *AtNOS/AtNOA1 is a functional Arabidopsis thaliana cGTPase and not a nitric-oxide synthase.* J Biol Chem, 2008. **283**(47): p. 32957-67.
111. Sakai, H., et al., *ARR1, a Transcription Factor for Genes Immediately Responsive to Cytokinins.* Science, 2001. **294**(5546): p. 1519-1521.
112. Hashim, Z., et al., *Metabolic profiling of retrograde pathway transcription factors rtg1 and rtg3 knockout yeast.* Metabolites, 2014. **4**(3): p. 580-98.
113. Harun, R., et al., *Bioprocess engineering of microalgae to produce a variety of consumer products.* Renewable and Sustainable Energy Reviews, 2010. **14**(3): p. 1037-1047.
114. Ruiz-Roig, C., et al., *The Hog1 SAPK controls the Rtg1/Rtg3 transcriptional complex activity by multiple regulatory mechanisms.* Mol Biol Cell, 2012. **23**(21): p. 4286-96.
115. Jazwinski, S.M. and A. Kriete, *The Yeast Retrograde Response as a Model of Intracellular Signaling of Mitochondrial Dysfunction.* Frontiers in Physiology, 2012. **Volume 3 - 2012**.
116. Torelli, N.Q., et al., *RTG1- and RTG2-dependent retrograde signaling controls mitochondrial activity and stress resistance in Saccharomyces cerevisiae.* Free Radical Biology and Medicine, 2015. **81**: p. 30-37.
117. Bajguz, A., *Brassinosteroids in Microalgae: Application for Growth Improvement and Protection Against Abiotic Stresses*, in *Brassinosteroids: Plant Growth and Development*, S. Hayat, et al., Editors. 2019, Springer Singapore: Singapore. p. 45-58.
118. Stirk, W.A., et al., *Endogenous brassinosteroids in microalgae exposed to salt and low temperature stress.* European Journal of Phycology, 2018. **53**(3): p. 273-279.